Studies on Cnidophage, Specialized Cell for Kleptocnida, of *Pteraeolidia semperi* (Mollusca: Gastropoda: Nudibranchia)

January 2021

Togawa Yumiko

Studies on Cnidophage, Specialized Cell for Kleptocnida, of *Pteraeolidia semperi* (Mollusca: Gastropoda: Nudibranchia)

A Dissertation Submitted to
the Graduate School of Life and Environmental Sciences,
the University of Tsukuba
in Partial Fulfillment of the Requirements
for the Degree of Doctor of Philosophy
(Doctoral Program in Life Sciences and Bioengineering)

Togawa Yumiko

Table of Contents

GENERAL INTRODUCTION

Generally, gastropods (Mollusca) have a calcareous shell that covers some to all of the upper surface of the animals. The molluscan's shell plays a defensive role against predators, which must contribute to their ecological success, although some gastropods have lost it (Bursca 2016). Members of the Opisthobranchia, namely sea slugs and allied molluscans, are characterized by their gills located posteriorly to heart unlike most of the other gastropods. The majority of opisthobranchian species have lost their shell partially or completely, and their exposed soft body parts often exhibit vivid coloration and/or peculiar morphology, which are thought to be involved in defense against natural enemies (Edmunds 1966). For example, *Chromodoris* sea slugs are known for their striking aposematic coloration presumably against visual predators (Zaccone 2019), which accumulate poisonous or distasteful chemicals obtained by feeding on sponges or algae (Faulkner and Ghiselin 1983). Other sea slug species are known for their Batesian mimicry, in which the non-poisonous species bear vivid coloration reminiscent of poisonous species, thereby avoiding predation (Edmunds 1966). On the other hand, inconspicuous coloration of many sea slugs, which is often derived from their food staff, seems to function as cryptic coloration (Wickler 1959; Faulkner and Ghiselin 1983; Edmunds 1987). Not only colors but also morphological traits are involved in defense and escape. For example, many cladobranchian sea slugs bear numerous dorsal protrusions called cerata, which are autotomized when attacked by enemies (Edmunds 1966). In addition, some cladobranchian species have evolved a unique defensive mechanism implemented in their dorsal cerata, called "kleptocnida".

Most cladobranchian sea slugs feed on cnidarians such as hydrozoans, sea anemones, jelly fish, etc. Nematocysts are cnidarian-specific cell organelles used for feeding and defense, whose capsular envelop contains a poisonous stinger thread that is discharged by mechanical or chemical stimuli (Ewer 1947). Strikingly, many sea slug species belonging to the Aeolidioidea have the ability to incorporate and store the food-derived nematocysts within the tip of the dorsal cerata, and the nematocyst-armored cerata are used for defense against enemies. This phenomenon is called "kleptocnida" or "nematocyst stealing" (Grosvenor 1903; Kepner 1943; Edmunds 1966). How the sea

slugs keep the nematocysts undigested, undischarged and stored is an enigma. It was suggested that the mucus of the sea slugs may have an activity to inhibit the nematocyst discharge, thereby enabling them to feed on cnidarians without injury (Greenwood 2004). Kleptocnida is an extremely unique and interesting phenomenon in that cell organelles of an organism are incorporated into other organism and function there, possibly representing an early stage of symbiosis. In this context, studies on the mechanism of kleptocnida is important in evolutionary biology. Previous attempts have shed some light on the mechanisms underlying kleptocnida. Histological studies revealed that the nematocysts are transported to the cnidosacs located at the tip of the cerata via the digestive gland, where the nematocysts are incorporated into the specialized cells for kleptocnida called the cnidophages (Grosvenor 1903; Martin 2003). It was proposed that the sea slugs can obtain and retain undischarged nematocysts by incorporating immature nematocysts into the cnidosacs and making them mature therein (Obermann et al. 2012), although this idea seems to be a mere hypothesis without solid evidence. At this stage, it is totally unknown how Aeolidioidea sea slugs can selectively incorporate and maintain intact nematocysts without digestion. According to the previous studies, the cnidophage is expected to play a role in selective incorporation and retention of the nematocysts. Hence, the basic characteristics of the cnidophage, such as developmental origin, ultrastructure, gene expression, etc. should be investigated in detail.

Thus far, no studies have collected and histologically inspected a sufficient number of immature cerata without cnidosacs and/or cnidophages. The main reason for the lack of knowledge is that rearing and maintenance of cladobranchian sea slugs are generally difficult. Recently, a long-term culturing method for the cladobranchian *Pteraeolidia semperi* has been established in our laboratory. In this study, therefore, I investigated *P. semperi*, which is large in size (up to 5 cm), easy to collect around the Misaki Marine Biological Station, Japan, and maintainable in the laboratory. First, focusing on the large number of dorsal cerata in which kleptocnida occurs, I investigated the formation and increase patterns of cerata during the growth of *P. semperi*, and found that the number of cerata continuously increases even in mature individuals, and the body regions where new cerata

are formed are predictable to some extent (Part I). Next, I attempted to get insight into the properties of cnidophage by examining the developmental process of cnidosacs and the detailed internal structure of cnidophages (Part II). Finally, I performed transcriptomic and proteomic analyses of the cnidosac samples using RNA-sequencing and mass spectrometry, thereby attempting to identify genes and proteins that are specifically up-regulated in cnidosac/cnidophage where kleptocnida occurs (Part III).

REFERENCES

Brusca RC, Moore W, Shuster SM (2016) Invertebrates. Sunderland, Massachusetts U.S.A: Sinauer Associates, Inc., Publishers

Edmunds M (1966) Protective mechanisms in the Eolidacea (Mollusca Nudibranchia). J Lin Soc Lond Zool 46: 27–71

Edmunds M (1987) Color in opisthobranchs. Am Malacol Bull 5: 185–196

Ewer RF, Fox HM (1947) On the functions and mode of action of the nematocysts of hydra. Proc Zool Soc Lond 117: 365–376

Faulkner DJ, and Ghiselin MT (1983) Chemical defense and evolutionary ecology of dorid nudibranchs and some other opisthobranch gastropods. Mar Ecol Prog Ser 13: 295–301

Greenwood PG, Garry K, Hunter A, Jennings M (2004) Adaptable defense: a nudibranch mucus inhibits nematocyst discharge and changes with prey type. Biol Bull 206: 113–120

Grosvenor G (1903) On the nematocysts of aeolids. Proc R Soc Lond. 72: 462–486

Kepner WA (1943) The manipulation of the nematocysts of *Pennaria tiarella* by *Aeolis pilata*. J Morphol 73: 297–311

Martin R (2003) Management of nematocysts in the alimentary tract and in cnidosacs of the aeolid nudibranch gastropod *Cratena peregrina.* Mar Biol 143: 533–541

Obermann D, Bickmeyer U, Wägele H (2012) Incorporated nematocysts in *Aeolidiella stephanieae* (Gastropoda, Opisthobranchia, Aeolidoidea) mature by acidification shown by the pH sensitive fluorescing alkaloid Ageladine A. Toxicon 60: 1108–1116

Winkler LR (1959) A mechanism of color variation operating in the West Coast sea hare, *Aplysia californica* Cooper. Pacific Sci 13: 63–66

Zaccone G (2019) Fish defenses. CRC Press

PART Ⅰ

Formation process of ceras rows in the cladobranchian sea slug *Pteraeolidia semperi*

INTRODUCTION

Sea slugs belonging to the Nudibranchia include more than 3,000 species, which form a shell-less clade in the molluscan class Gastropoda (Thompson 1976; Wägele and Willan 2000; Wägele amd Klussmann-Kolb 2005). Sea slugs are famous for their striking diversity in color and morphology, which are represented by, for example, vivid warning coloration and sophisticated camouflage (Wägele and Klussmann-Kolb 2005; Putz 2010). Some species belonging to the Cladobranchia, a clade of the Nudibranchia, possess a number of projections called “cerata” on their back, which can be detached by autotomy to avoid predatory attacks (Bickell-Page 1989; Edmunds 1966). Some cladobranchian sea slugs, which mainly feed on hydrozoans, sea anemones and other cnidarians, are also known for an intriguing phenomenon so-called “kleptocnida” or “cleptocnida”. Tentacles of cnidarian animals contain specialized cells for predation and defense called “nematocytes”, “cnidocytes” or “cnidoblasts”, which contain giant subcellular organelles called “nematocysts”, “cnidocysts” or “cnidae” with harpoon-like structure and toxin-injecting function (Kass-Simon and Scappaticci 2002). The sea slugs feed on the cnidarians, and strikingly, only the nematocysts remain undigested, being incorporated into and accumulated within the cerata with keeping the toxin-injecting functionality (Grosvenor 1903; Greenwood 2009). The “stolen nematocysts” stored in the cerata are believed to be utilized by the sea slugs for defensive purposes (Edmunds 2009). In addition to the defensive roles, the cerata of the sea slugs may be involved in other biological functions such as facilitating the respiration by increasing epidermal surface area, and promoting the photosynthesis by harboring symbiotic zooxanthellae (Rudman 1982; Herdman 1890; Edmunds 2009). Developmental aspects of these fascinating morphological traits in the cladobranchian sea slugs have been poorly understood.

In an attempt to understand the process of ceras formation, I investigated the postembryonic development of a cladobranchian sea slug *Pteraeolidia semperi* (Bergh 1870), which is called "Mukadé Mino-Umiushi" (= centipede-like cladobranchian sea slug) in Japanese. This species is found in subtidal rocky zones ranging from Japan, Southeast Asia, Pacific islands to Hawaii (Bergh 1870; Wilson and Burghardt 2015). A recent genetic study using molecular markers uncovered the presence of several genetically-distinct groups in *P. samperi*, which might be regarded as different species (Yorifuji et al. 2012). *P. samperi* possesses numerous cerata on the dorsal side, whose body size is relatively large, sometimes reaching up to 70 mm. I collected *P. semperi* individuals representing a variety of postembryonic developmental stages (**Fig. 1-1**), and recorded their body length, number of cerata and ceras morphology, and analyzed the increasing patterns of ceras number and the changing patterns of ceras morphology.

MATERIALS AND METHODS

Sample collection

Individuals of *P. semperi* were collected once or twice per month from July to September in 2018 by snorkeling at subtidal rocky areas in Kanagawa and Chiba prefectures, Japan. The collected animals were kept in an aquarium (35 cm × 35 cm × 30 cm) with seawater circulated through a filter pump at 18.5°C. The animals were fed with hydrozoans, *Tubularia* spp., commonly found at the sampling localities ad libitum by introducing and replacing field-collected rocks on which the hydrozoans grew.

Size measurement

The collected animals were individually placed in a petri dish and photographed when they were the most relaxed. The body size parameters measured were defined as shown in **Fig. 1-2A**. A digital camera attached on a stereomicroscope (SZX-16; Olympus, Tokyo, Japan) was used for photographing the individuals smaller than 30 mm in body length. A digital camera (WG-50; Richo Co.Ltd., Tokyo, Japan) was used for photographing the individuals 30 mm or larger in body length. After taking the photos, the individuals were fixed with Bouin solution. Body length, head width, number of cerata, and number of ceras rows (see **Fig. 1-2A**) were measured on the photographs by using the ImageJ software (National Institutes of Health, Bethesda, Maryland, USA). Whether or not each ceras cluster accompanies the glove-like structure was also diagnosed from the photographs. The glove-like structure was judged to be present when both of the following characteristics were found on a single ceras cluster; the presence of bulge between the body trunk and the cerata and the clear borderline between the bulge and the basal parts of the cerata (**Fig. 1-3B**).

Allometric analysis

Allometric changes during the postembryonic development were quantified to understand the growth patterns, where the body length was used as the growth indicator instead of age, since it was difficult to infer the age of the collected animals. The body length ratio relative to the head width, the total

number of cerata, and the number of ceras rows in a single individual were analyzed by using the following models.

Linear model:

$$D = \alpha L + \beta$$

Allometric model:

$$D = \alpha L^{\beta}$$

Logistic model:

$$D = \frac{D_{\infty}}{1 + e^{-k(L-L_0)}}$$

where the L is the body length, and the D indicates dependent variables such as the relative head width, the total number of cerata and the number of ceras rows. The α and β are the parameters of the two models, the linear and the allometric models. The D_{∞} is the parameter indicating the limit value of the dependent variable D. The L_0 is the parameter indicating the estimated body length when the D becomes zero. The k is the parameter showing the degree changing the D in response to the body length L in the logistic model. All the parameters were estimated by the least-squares method with the Excel 2011 (Microsoft, Redmond, WA, USA). The best model was selected in accordance with the Akaike's Information Criterion (AIC).

The relationship between the body length and the percentage of the ceras rows with glove-like structure in the total ceras rows per individual was analyzed with the logistic model using the generalized linear model (GLM) with binominal distribution and logit transformation. The significance of the parameters was examined by the Wald test. To estimate the effect of the presence of the basal bulge for the number of cerata in a single ceras cluster, the relationship between the number of cerata in a single ceras cluster and the other body size-dependent factors were analyzed by the GLM with gaussian distribution and no data transformation after standardizing all the data. By standardizing the data, the scales of the data become the same, enabling to compare the influence degree among the

variables. The body length, the total number of ceras rows, the order of the target ceras cluster from the anterior side and the presence of the basal bulge in the target ceras cluster were used as the independent variables for the analysis. The best model was determined in accordance with the AIC values by using the step function as described above. The significance of the parameters was examined by the Wald test. The influence degrees of the respective variables were evaluated with the standardized partial coefficients through the analysis. To determine whether the glove-like ceras clusters are formed from anterior or posterior side in the body trunk as the body size increases, the relationship between the presence of the basal bulge in a single ceras cluster and the other factors were analyzed by the GLM with binominal distribution and logit transformation. Then, standardized data of the body length, the total number of ceras rows and the number of ceras in the respective ceras rows were used as independent variables for explaining that. The best model was selected in accordance with AIC by using the step function in the R software ver. 3.4.2 (R Core Team 2017). The significance of the parameters was examined by the Wald test. These statistical analyses were performed using the R software ver. 3.4.2 (R Core Team 2017).

Size comparison of the basal bulges and other parts in the glove-like ceras clusters

To assess the importance of the basal bulge as a place for putting more cerata, the size of the perimeter lengths of the basal bulges, the basal part of the basal bulge and the body trunk were measured in the Bouin fixed samples. The animals having glove-like structures in all ceras rows were selected for the comparison. The samples were cross-sectioned and taken photos for the measurement of respective target lengths. The respective sizes were measured from the photos by using the ImageJ software (National Institutes of Health). Then, the second ceras cluster was chosen for the measurement as the most sufficiently developed ceras cluster. The first one was not targeted since the first one often showed different morphologies comparing to the others. The significance of the difference of means was examined by the Welch's *t*-test after testing the homoscedasticity by the *F*-test.

Simulation for increase of ceras number

A simulation was performed to estimate how formation of the basal bulge can influence the total number of cerata. A base model explaining the number of cerata in a single cluster for the simulation was made as the first step. The relationship between the number of cerata in a single ceras cluster and the other body factors were analyzed by the GLM with Poisson distribution and log transformation without standardizing data. The body length, the total number of ceras rows, the order of the target ceras cluster from the anterior side and the presence of the basal bulge in the target ceras cluster were used as the independent variables. The best model was determined in accordance with AIC by using the step function in the R software ver. 3.4.2 (R Core Team 2017). The following model explaining the number of cerata at a single ceras cluster was accordingly obtained:

$$N_i = e^{\alpha C_{total} + \beta \frac{i}{C_{total}} + \gamma G_i + c} \qquad (1)$$

where the i is the order of ceras rows counted from the anterior side, and the N_i is the number of cerata at the ceras rows i. The C_{total} is the total number of ceras rows, and the G_i indicates the presence of the basal bulge making the ceras cluster glove-like. The e is Napier's constant. The α, β, γ and c are the parameters whose values were estimated through the GLM analysis above (**Table 1-1**). The total number of ceras rows C_{total} can be estimated from the body length L with the logistic mode using the parameter values estimated in the allometric analysis above:

$$C_{total} = \frac{C_\infty}{1 + e^{-k_C(L - L_{c \cdot 0})}} \qquad (2)$$

where the C_∞ is the max number of the total ceras rows in a single individual. The $L_{c \cdot 0}$ is the logically estimated body length when the number of total ceras rows C_{total} becomes zero. The k_c is the parameter showing the degree changing the C_{total} in response to the body length L in the model. The number of ceras rows with glove-like clusters in a single individual can be estimated by the following models:

$$G_{total} = C_{total} \times G_p \qquad (3)$$

$$G_p = \frac{1}{1 + e^{-k_g(L - L_{g \cdot 0})}} \qquad (4)$$

where the G_{total} is the total number of the total ceras rows with glove-like clusters, and the G_p is the

percentage of the number of ceras rows with glove-like clusters in total number of ceras rows. The $L_{k\cdot 0}$ is the logically estimated body length when the G_p becomes zero. The k_g is the parameter showing the degree changing the G_p in response to the body length L in the model. According to the results by the allometric analysis above, the parameter for the order of ceras rows counted from anterior side was minus (**Table 1-2**), indicating that whether or not a cluster becomes glove-like is negatively affected as the order goes from anterior to posterior. In other words, that indicates that the ceras clusters become glove-like from anterior to posterior as the body size becomes larger. Based on that, it can be considered that the ceras clusters with glove-like structures locate at the ceras rows until the order G_{total} counted from the anterior side. Accordingly, the presence of the glove-like ceras cluster at the ceras row order i can be estimated as follow.

$$G_i = \begin{cases} 1 \ (G_{total} \geq i) \\ 0 \ (G_{total} < i) \end{cases} \qquad (5)$$

where the G_i is the presence of the glove-like structure on the target single ceras row. By substituting the models (2)–(5) into the model (1), N_i which is the number of cerata at the ceras row order i can be estimated from the body length L. The total number of cerata in a single individual N_{total} can be estimated by the following calculation.

$$N_{total} = \sum_{i=1}^{C_{total}} N_i \qquad (6)$$

In this study, the total number of cerata N_{total} was estimated by changing the body size L with 5 mm of intervals. The changes of the total number of cerata in normal ceras formation pattern was simulated with using all the models above as a control. Thereafter, the situation if *P. semperi* did not acquire the body plan making glove-like ceras clusters in the evolutionary process was simulated by substituting zero to the G_i under any conditions. The importance of making the ceras clusters glove-like in having more cerata on the body was determined through these simulations. All the simulations were performed with the Excel 2011 (Microsoft).

RESULTS AND DISCUSSION

Collected individuals of *P. semperi*

At subtidal rocky areas in Kanagawa and Chiba Prefectures, Japan, 69 individuals of *P. semperi* were collected. Their body length ranged from 3 mm to 47 mm. Smaller individuals tended to possess fewer cerata with pale and whitish body color (**Fig. 1-1A, B**), while larger individuals possessed numerous cerata whose body color was blue, purplish blue, or sometimes brownish (**Fig. 1-1C, D**). The age-dependent color variation is probably relevant to the presence of symbiotic zooxanthellae (Rudman 1982).

Allometric change during growth

In general, proportion of body parts, i.e., allometry, can change through the growth of animals (Huxley and Teissier 1936; Stern and Emlen 1999; Damuth 2001). Therefore, not only the size of animal body but also its allometric change can be an indicator for staging the animal growth. Hence, I analyzed the ratio of the body length to the head width using the individuals of different body sizes. The body length ratio to the head width increased as the body length increased in individuals smaller than 20 mm, and it reached a plateau in larger individuals (**Fig. 1-2B**). Based on the AIC model selection, logistic model was chosen for the relationship (**Table 1-3**), suggesting that the body length ratio to the head width increases at early stages but gradually approaches to a certain proportion at later stages. These results also suggest the possibility that the postembryonic development of *P. semperi* may be divided into two phases, i.e., the immature growth phase and the mature growth phase.

Increase of total ceras number

The total number of cerata per individual was shown to increase as the body length increased (**Fig. 1-2C**). The pattern of increase fitted to the logistic model (**Table 1-3**). The number of cerata was shown to increase drastically in the individuals of 10-30 mm in body length. Based on the logistic model, the maximum cerata number was inferred as 270. Based on our observations in this study, the actual

maximum was 280 cerata per individual.

Formation and increase of ceras rows

The cerata on the dorsal side exhibited a conspicuous formation of the repeated and laterally-paired clusters or rows along the antero-posterior axis of the animals (**Fig. 1-2A**). The number of ceras rows increased as the body length of the animals increased, and the pattern fitted to the logistic model (**Fig. 1-3A, Table 1-3**). It reached a plateau at around 15 rows, where the body length was around 27 mm. Notably, this pattern did not agree with the pattern regarding the total number of cerata, which did not look like attaining an upper limit even in the animals of over 30 mm in body length (**Fig. 1-2C**). These results indicate that the number of cerata per row increases even after the formation of new ceras rows stops.

Formation of basal bulge and glove-like structure

I found that a structural transformation of each ceras cluster (= a side of each ceras row) accounts for the above-mentioned pattern that the number of cerata per row increases even after the formation of new ceras rows stops (cf. **Fig. 1-2C**, **Fig. 1-3A**). In the well-developed ceras clusters, their basal region was swollen to form a bulge. From the bulge, multiple cerata radially projected, where the boundary between the bulge and each ceras was clearly seen (**Fig. 1-3B (a, c)**). In the less-developed ceras clusters, by contrast, their basal region lacked the bulge (**Fig. 1-3B (b, d)**). This "glove-like structure" consisting of the basal bulge and the radially-protruding cerata tended to be observed in larger animals. When the proportion of ceras rows with the glove-like structure to the total number of ceras rows was plotted against the body length, a near-sigmoidal pattern emerged (**Fig. 1-3C**). In detail, (i) tiny individuals smaller than 10 mm lacked the glove-like structure, (ii) the glove-like structure appeared in individuals larger than 10 mm, (iii) the glove-like structure was found in the majority of individuals larger than 15 mm, and (iv) most of the ceras rows accompanied the glove-like structure in individuals larger than 30 mm.

Contribution of basal bulge and glove-like structure to increased number of cerata

These observations suggested that the formation of basal bulge and resultant glove-like structure may contribute to the increase of ceras number even after the number of ceras rows reached the plateau. Actually, for example, when two individuals of similar size but with different levels of bulge formation were compared, a 14 mm individual with 13 ceras rows, of which 11 rows (85%) developed the basal bulge, was with 180 cerata in total (**Fig. 1-3D (a)**), whereas a 11 mm individual with 11 ceras rows, of which no row (0%) exhibited the basal bulge, was with only 52 cerata in total (**Fig. 1-3D (b)**).

In order to evaluate these patterns statistically, I performed the GLM analysis with the standardized data to explain the number of cerata on a single cluster (one side of a row pair). It was demonstrated that the absolute value of standardized coefficient for the parameter showing the presence of glove structure was the largest in the best model (**Table 1-4**), implying that the presence of basal bulge and resultant glove-like structure has the largest effect on the ceras number per cluster among the parameters examined. Considering the morphology of the glove-like structure, the basal bulge is likely to function as the basis for ceras formation. By swelling the epidermis of the body trunk, the basal area for ceras formation is enlarged, thereby enabling to increase the ceras number.

In an attempt to test this idea theoretically, I performed a simulation study in which the patterns of ceras formation were compared between the conditions with and without the basal bulge. Under the realistic conditions I adopted (see Materials and Methods), the total number of cerata in the absence of the basal bulge was less than a half of the number of cerata in the presence of the basal bulge (**Fig. 1-4**), reinforcing the results of morphological observations (see **Fig. 1-3D**) and statistical analysis (see **Table 1-4**).

On functional significance of increased ceras number

These results strongly suggest that, during the postembryonic development of *P. semperi*, the increase of dorsal cerata entails the following processes: (i) increase of the number of ceras rows, (ii) formation

of the basal bulge in each ceras cluster, and (iii) increase of the number of cerata per ceras cluster. As a consequence, well-grown individuals of *P. semperi* may possess over 270 cerata on the dorsal side. Conceivably, developing a large number of cerata should be beneficial for the sea slugs via such biological functions as defense against enemies by kleptocnida, enhanced gas exchange by increasing epidermal surface area, and photosynthesis by harboring symbiotic zooxanthellae (Rudman 1982; Herdman 1890; Edmunds 2009).

Conclusion and perspective

In this study, I described the development and morphogenesis of *P. semperi* in unprecedented detail, with special focus on the formation and increase of the dorsal cerata. **Figure 1-5** summarizes the results, which highlights 4 developmental phases roughly represented by animal size classes, and 4 morphogenetic processes, namely the growth and elongation of body shape, the increase of ceras number, the increase of ceras rows, and the development of glove-like structure to increase the number of cerata per cluster. Considering that morphology, number, orientation and distribution of the dorsal cerata are diverse among different cladobranchian species (Goodheart et al. 2017; Goodheart et al. 2018), whether the patterns observed in *P. semperi* also apply to other cladobranchians is of interest and to be examined in future studies.

Because cladobranchian sea slugs are generally not easy to be maintained in the laboratory for an extended period, previous developmental and morphogenetic studies on them have been limited and fragmentary (Thompson and Bennett 1970; Miller 1977; Rudman 1982; Hoegh-Guldberg and Hinde 1986; Caballer and Ortea 2015; Goodheart et al. 2017; Goodheart et al. 2018). I am particularly interested in the development, morphogenesis, gene expression, and cellular and molecular biology of the dorsal cerata in cladobranchians because these structures are involved in such exciting phenomena as kleptocnida and symbiotic photosynthesis (Rudman 1982; Schmitt and Wägele 2011). To that end, I am currently working on the establishment of a continuous rearing system for *P. semperi* in the laboratory, the examination of histological, cytological, biochemical and transcriptomic aspects of the

dorsal cerata, and the development of molecular and genetic tools applicable to the cladobranchian species.

REFERENCES

Bergh LSR (1870) Malacologische Untersuchungen. Reisen im Archipel der Philippinen 1: 315-344

Bickell-Page LR (1989) Autotomy of cerata by the nudibranch *Melibe Leonina* (Mollusca): Ultrastructure of the autotomy plane and neural correlate of the behaviour. Phil Trans R Soc Lond B 324: 149-172

Caballer M, Ortea J (2015) Finishing to untangling the taxonomic knot: new species of the genus *Bulbaeolidia* Carmona, Pola, Gosliner & Cervera, 2013 (Mollusca: Aeolidiidae) from the Caribbean and Galapagos. Rev Acad Canar Cienc 27: 113-123

Damuth J (2001) Scaling of growth: Plants and animals are not so different. Proc Natl Acad Sci USA 98: 2113–2114

Edmunds M (1966) Defensive adaptations of *Stiliger vanellus* Marcus, with a discussion on the evolution of 'nudibranch' molluscs. J Molluscan Stud 37: 73–81

Edmunds M (2009) Do nematocysts sequestered by aeolid nudibranchs deter predators? – a background to the debate. J Molluscan Stud 75: 203–205

Goodheart JA, Bazinet AL, Valdés Á, Collins AG & Cummings MP (2017) Prey preference follows phylogeny: Evolutionary dietary patterns within the marine gastropod group Cladobranchia (Gastropoda: Heterobranchia: Nudibranchia). BMC Evol Biol 17: 1–14

Goodheart JA, S Bleidißel, Dorothee Schillo, Strong EE, DL Ayres, A Preisfeld, AG Collins, MP Cummings, H Wägele (2018) Comparative morphology and evolution of the cnidosac in Cladobranchia (Gastropoda: Heterobranchia: Nudibranchia). Front Zool 15: 1–18

Greenwood PG (2009) Acquisition and use of nematocysts by cnidarian predators. Toxicon 54: 1065–1070

Grosvenor GH (1903) On the nematocysts of aeolids. Proc R Soc Lond 72: 462-486

Herdman WA (1890) On the structure and functions of the cerata or dorsal papillae in some nudibranchiate mollusca. Quart J Microscop Sci 31: 41-63

Hoegh-Guldberg O, Hinde R (1986) Studies on a nudibranch that contains zooxanhellae I. Photosynthesis, respiration and the translocation of newly fixed carbon by zooxanthellae in *Pteraeolidia ianthina*. Proc R Soc Lond B 228: 493-509

Huxley JS, Teissier G (1936) Terminology of relative growth. Nature 137: 780–781

Kass-Simon G, Scappaticci AA Jr (2002) The behavioral and developmental physiology of nematocysts. Can J Zool 80: 1772–1794

Miller MC (1977) Aeolid nudibranchs (Gastropoda: Opisthobranchia) of the family Tergipedidae from New Zealand waters. Zool J Linn Soc 60: 197-222

Putz A, Köning GM, Wägele H (2010) Defensive strategies of Cladobranchia (Gastropoda, Opithobranchia). Nat Prod Rep 27: 1386-1402

R Core Team (2017) R: A Language and Environment for Statistical Computing. https://www.R-project.org/

Rudman WB (1982) The taxonomy and biology of further aeolidacean and amerinacean nudibranch molluscs with symbiotic zooxanthellae. Zool J Linn Soc 74: 147-196

Schmitt V, Wägele H (2011) Behavioral adaptations in relation to long-term retention of endosymbiotic chloroplasts in the sea slug *Elysia timida* (Opisthobranchia, Sacoglossa). Thalassas 27: 225-238

Stern DL, Emlen DJ (1999) The developmental basis for allometry in insects. Development 126: 1091-1101

Thompson TE, Bennett I (1970) Observations on Australian Glaucidae (Mollusca: Opisthobranchia). Zool J Linn Soc 49: 187-197

Thompson TE (1976) Biology of Opithobranch Molluscus
Vol. I. London: The Ray Soc

Wägele H, Klussmann-Kolb A (2005) Opisthobranchia (Mollusca, Gastropoda) - More than just slimy slugs. Shell reduction and its implications on defence and foraging. Front Zool 2: 1–18

Wägele H, Willan RC (2000) Phylogeny of the Nudibranchia. Zool J Linn Soc 130: 83–181

Wilson NG, Burghardt I (2015) Here be dragons – phylogeography of *Pteraeolidia ianthina* (Angas, 1864) reveals multiple species of photosynthetic nudibranchs (Aeolidina: Nudibranchia). Zool J Linn Soc 175: 119-133

Yorifuji M, Takeshima H, Mabuchi K, Nishida M (2012) Hidden diversity in a reef-dwelling sea slug, *Pteraeolidia ianthina* (Nudibranchia, Aeolidina), in the Northwestern Pacific Zool Sci 29: 359-367

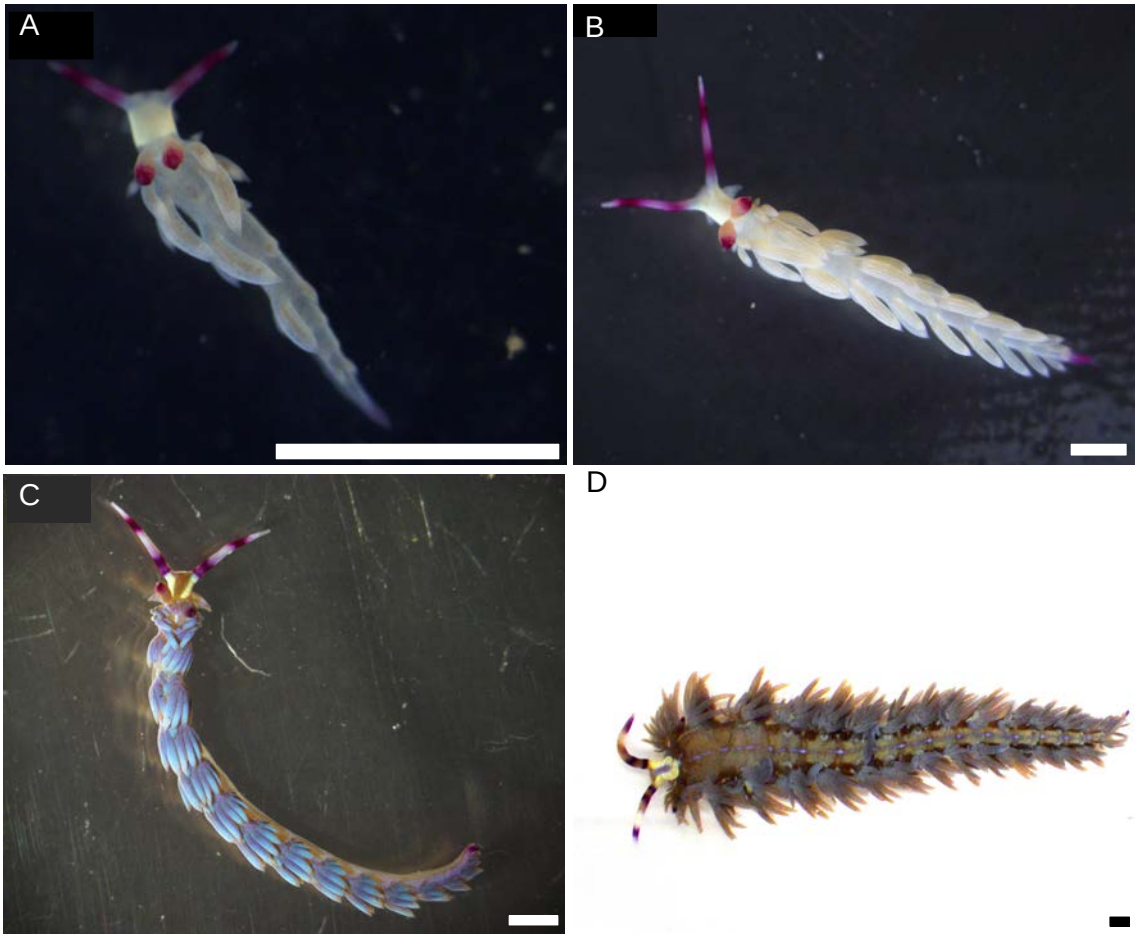

Fig.1

Fig. 1-1. External morphology of *P. semperi* individuals of different body size. (A) A 3-mm individual collected at Kanagawa on 13 July 2018. The body is whitish in color with only a small number of cerata that are not yet symmetrically arranged. (B) A 9-mm individual collected at Chiba on 10 July 2018. The body is whitish in color with symmetrically positioned cerata. (C) A 29-mm individual collected at Kanagawa on 26 August 2018. The body is bluish or purplish in color with a large number of cerata. (D) A 47-mm individual collected at Kanagawa on 13 September 2018. The brownish body color is probably attributed to the proliferation of symbiotic zooxanthellae. The glove-like structure at the base of each ceras cluster is evidently seen. All scale bars indicate 2 mm.

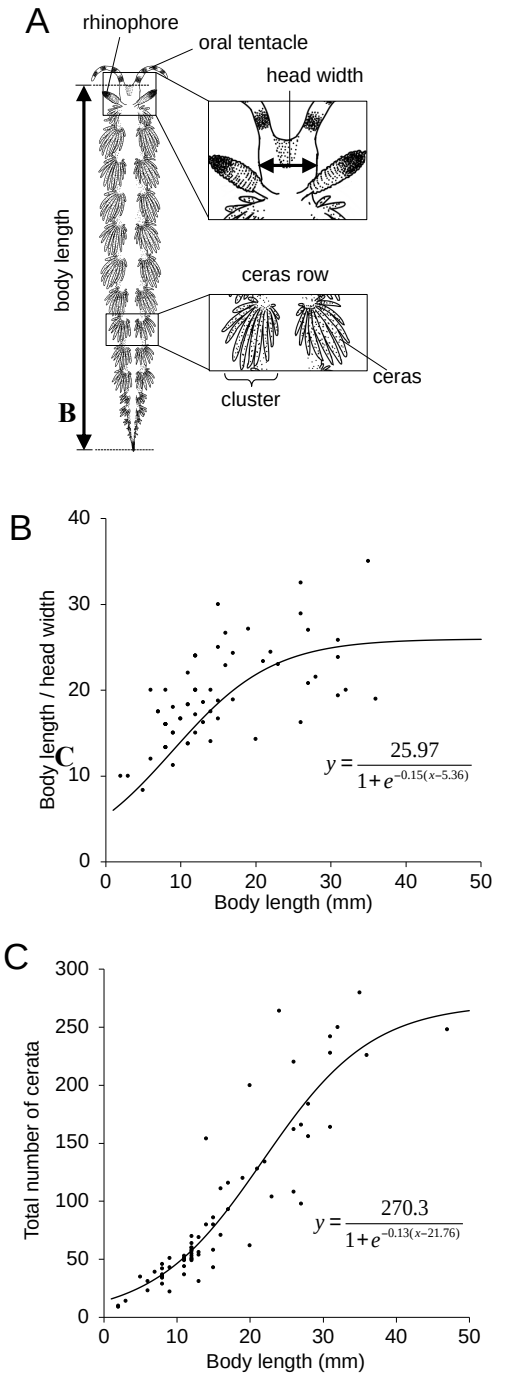

Fig. 1-2. Relationships between body size, allometry and number of cerata of cerata in *P. semperi*. (A) Morphological parameters of *P. semperi* inspected and measured in this study. (B) Relationship of the proportion of the body length relative to the head width plotted against the body length, which illustrates the allometric change in the body proportion during the growth of *P. semperi*. The logistic model was selected as the best model in accordance with AIC, as shown in Table 3 (n = 65; R^2 = 0.46; AIC = 386.0). These results indicate that the length/width ratio is initially small and becomes larger as the animals grow, and finally reaches a plateau in full-grown animals. (C) Relationship between the total ceras num- ber and the body length in *P. semperi*. The logistic model was selected as the best model in accordance with AIC, as shown in Table 3 (n = 69; R^2 = 0.83; AIC = 669.1). The total ceras number shows a sigmoidal increase with the body growth, suggesting that the total ceras number may have a sort of upper limit.

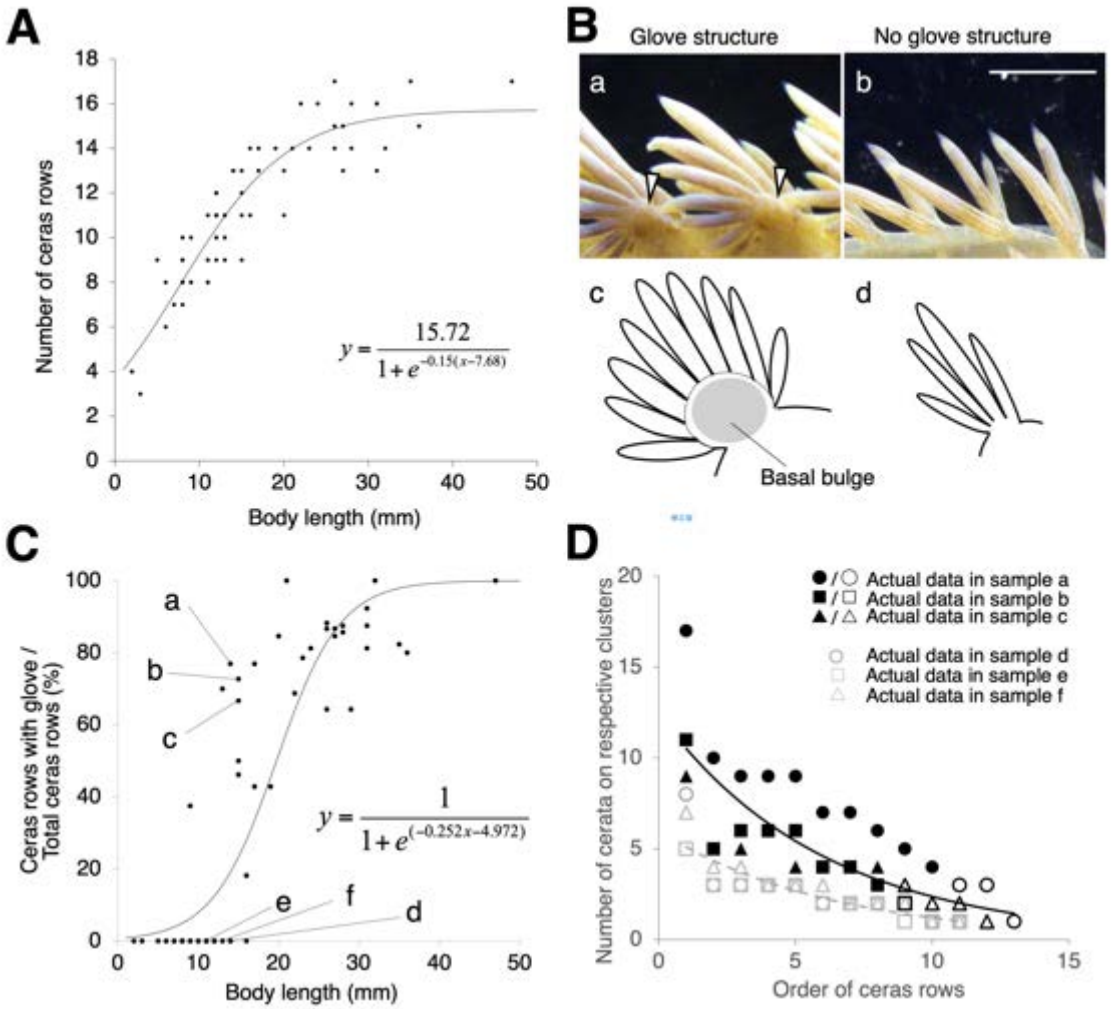

Fig. 1-3. Morphological changes of ceras clusters, and comparison of ceras numbers between different types of ceras clusters (i.e., with/without glove-like structures). (A) Relationship between the number of ceras rows and the body length. The logistic model was selected as the best model in accordance with AIC, as shown in Table 3 (n = 69; R^2 = 0.84; AIC = 228.2). Initially the number of ceras rows linearly increases, and reaches a plateau at around 20–30 mm of the body length. (B) Morphology of ceras clusters with and without the glove-like structure. Note that the ceras cluster with the glove-like structure (a) bears a greater number of cerata than the ceras cluster without the structure (b). White arrowheads indicate the basal bulge of the structure. Schematic drawings of the respective types of the ceras clusters are shown below (c, d). The scale bar shows 2 mm. (C) Ratios of the number of ceras clusters bearing the glove-like structure to the total number of ceras clusters plotted against the body length, which shows a sigmoidal curve (n = 68; R^2 = 0.76; Wald test; $P < 0.05$). The glove-like structure initially appears at around 10 mm of body length, and almost all of the ceras clusters bear the structure at around 30 mm of body length. Alphabets in the graph indicate the individuals with (a–c) or without (d–f) glove-like structures, that were further analyzed in D. (D) Relationship between the number of ceras and the position of ceras rows in six individuals of similar body sizes, with or without glove-like structures. The alphabets in the legend show the individuals that correspond to those in (C). Filled plots indicate ceras clusters with the glove-like structure, while open plots show the ceras clusters without the structures.

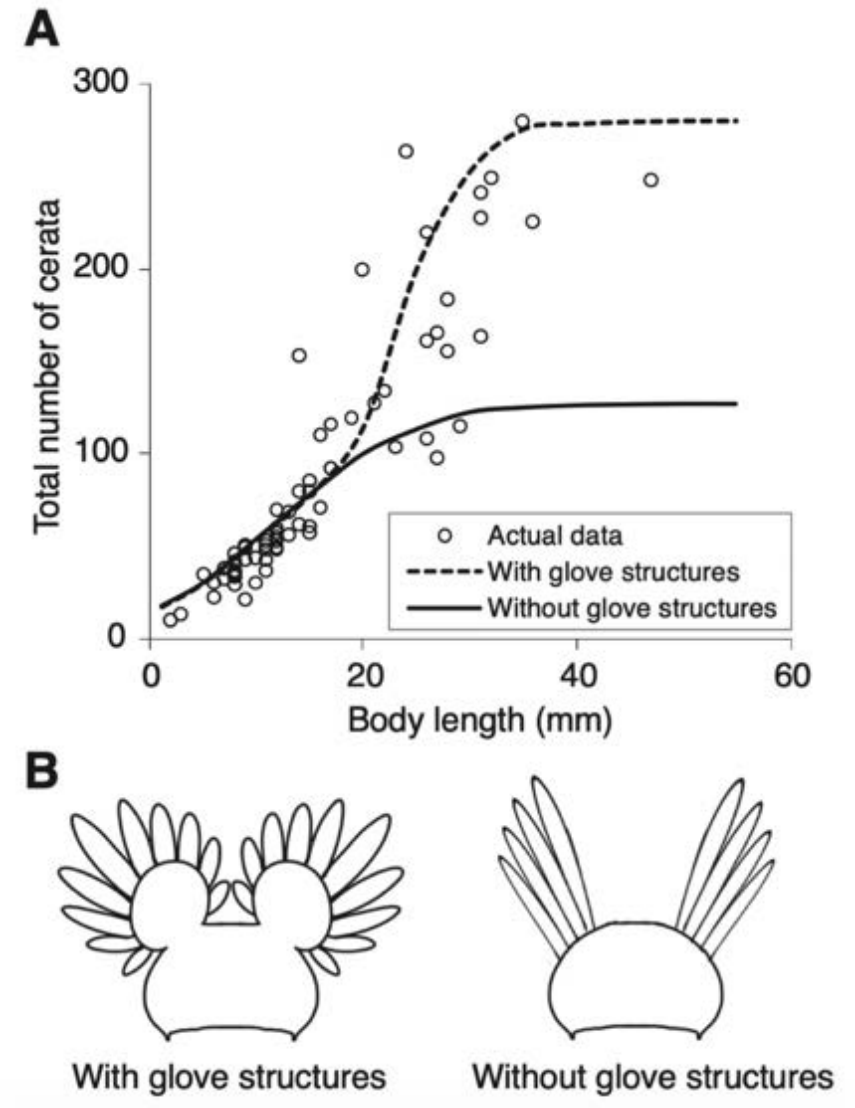

Fig. 1-4. Simulation on hypothetical role of glove-like structure for ceras formation. (A) Change of the total ceras number in a single simulated individual. The solid line indicates the total number of cerata under the constraint of no formation of the glove-like structure. The dotted line indicates the total number of cerata under the condition that formation of the glove-like structure is allowed. While the total number of cerata reaches a plateau in both cases, the maximal number of cerata in the individual without the glove-like structures was less than a half of that in the individual with the glove-like structures. (B) Schematic drawings of the cross-sectional views of the body trunk of the simulated individuals at the position with ceras rows. Left, with the glove-like structure; right, without the glove-like structure. Note that the basal bulge of the glove-like structure increases the area on which the cerata are arranged, which enables formation of a larger number of cerata.

Phase 1	Phase 2	Phase 3	Phase 4
under 10 mm	10 ~ 20 mm	20 ~ 30 mm	over 30 mm
			
Increase of cerata			
Body proportion changes			
Increase of ceras rows			
	Increase of glove structure		

Fig. 1-5. Summary of morphological changes during growth of *P. semperi.*

Table 1-1. AIC and coefficients of the top two models to explain the number of cerata on a single cluster. These estimated parameters were used for the simulation in Figure 4. Asterisks indicate statistical significances (n = 20; Wald test; $p < 0.05$).

	AIC	ΔAIC	Parameters (SE)				
			Intercept	Body length	Total number of ceras rows	Order of ceras rows / total number of ceras rows	Glove structure
Model 1	1059.6	0	1.249* (0.137)	-	0.0485* (0.0107)	-0.0122 (0.000924)	0.789* (0.0804)
Model 2	1061.3	1.7	1.218* (0.149)	-0.00246 (0.00458)	0.0545* (0.0154)	-0.0122* (0.000925)	0.801* (0.0832)

Table 1-2. Standardized partial regression coefficients of the best models to explain the presence of glove structure. Asterisks indicate statistical significances (n = 20; Wald test; $p < 0.05$).

Parameters (SE)			
Intercept	Body length	Total number of ceras rows	Order of ceras rows / total number of ceras rows
1.154*	1.284*	1.351*	-0.872*
(0.230)	(0.404)	(0.479)	(0.208)

Table 1-3. AIC and R^2 values which were calculated on respective regression models for the relations between body length and body length / head width, total number of cerata or number of ceras rows. The lowest values of AIC or the highest R^2 values are expressed as bold.

Model	Body length / head width vs. body length		Total number of cerata vs. body length		Number of ceras rows vs. body length	
	AIC	R^2	AIC	R^2	AIC	R^2
Linear	390.2	0.40	673.9	0.81	259.56	0.74
Allometric	386.3	0.44	679.4	0.79	240.17	0.81
Logistic	**386.0**	**0.46**	**669.1**	**0.83**	**228.2**	**0.84**

Table 1-4. AIC and standardized partial regression coefficients of the top two models to explain the number of cerata on a single cluster. Asterisks indicate statistical significances (n = 20; Wald test; $p < 0.05$).

	AIC	ΔAIC	Parameters (SE)				
			Intercept	Body length	Total number of ceras rows	Order of ceras rows / total number of ceras rows	Glove structure
Model 1	412.5	0	-0.511* (0.0696)	-	0.250* (0.0454)	-0.510* (0.0364)	0.810* (0.0957)
Model 2	414.5	2.0	-0.509* (0.0720)	0.0111 (0.0706)	0.241* (0.0693)	-0.511* (0.0367)	0.805* (0.1000)

Part Ⅱ

Development, regeneration and ultrastructure of ceras, cnidosac and cnidophage, specialized organ, tissue and cell for kleptocnida in *Pteraeolidia semperi*

INTRODUCTION

The digestive organ of the gastropods is dominated by the digestive glands. The digestive glands of *P. semperi* are finely branched into digestive diverticula, which are generally constituted by two types of cells, the digestive cells and the basophilic cells (Voltzow 1994). Foods ingested by the gastropods are subjected to extracellular digestion, and the resultant food particles are taken up by the digestive cells and completely digested by lysosomes. However, in some sea slugs that feed on cnidarians and perform kleptocnida, only the nematocysts, or cnidae, are not digested and transported into the specialized structures located at the tip of the digestive diverticula, called the cnidosacs, where they are retained and utilized for defense. Therefore, the cnidosacs are considered to be important for kleptocnida (Goodheart et al. 2018).

The inner surface of the cnidosac is lined with characteristic cells called cnidophages, and food-derived nematocysts are taken up by and retained in these cells (Greenwood and Mariscal 1984). The fact that the cnidophages specifically take up and retain nematocysts without digesting them has been histologically shown in several previous studies (Martin 2003; Goodheart et al. 2018). On the ground that the cnidophages may selectively incorporate specific types of nematocysts (Kepner 1943; Day and Harris 1978), it was speculated that the cnidophages might possess receptors that specifically recognize the nematocysts, but no evidence has been provided yet. In order to understand the mechanisms underlying kleptocnida, it is pivotal to understand the cellular and other biological aspects of the cnidophages.

In this study, I carried out detailed observations of the process of the cnidophage differentiation at the tip of the digestive diverticula in *P. semperi*. The morphology of the cnidophage was clearly

distinguishable from the digestive cells based on the size of cytoplasm. Then, I described the process as to how the specialized cells in the cnidosac differentiate from the normal gastrointestinal epithelial cells. In this chapter, based on my observations that new cerata are formed on the tail region and the glove edges in *P. semperi*, I sampled and observed the newly formed cerata by focusing on the tail of the individual and the base of the glove structure. In addition, considering that it is not easy to observe the development process of naturally-developing cerata in a chronological order, I also observed the experimentally induced regeneration process of cerata. There is a report about regeneration of cerata after autotomy in a cladobranchian sea slug *Phidiana crassicornis*, in which a new ceras was formed at the autotomized site, and a cnidosac was formed in parallel with the elongation of the regenerating ceras (Miller and Byrne 2005). Inspired by the previous study, I excised the tips of the cerata containing the cnidosacs from *P. semperi*, sampled the regenerating cerata everyday since the operation, and performed histological inspection of the regenerating cerata specimens. In addition, while several previous studies observed the incorporation process of the nematocysts into the cnidophages by transmission electron microscopy (TEM) (Greenwood and Mariscal 1984; Martin 2003; Martin et al. 2009), more detailed ultrastructural descriptions of the cnidophages are anticipated. In this study, therefore, I also observed the cnidophages of *P. semperi* using TEM, and described the ultrastructure in detail.

MATERIALS AND METHODS

Sample collection

In order to observe the initial formation process of cerata, tiny protrusions, about 100 μm in size, on the tail of the *P. semperi* (**Fig. 2-1 bottom; Fig. 2-2A**), and also small protrusions, about 300 μm or less in size, on the base of the glove structures (**Fig. 2-1 bottom**) were collected from *P. semperi*. In the regeneration experiment, the tips of the cerata, 1 mm or longer in size and considered to be sufficiently mature, on the anterior glove structures were excised (**Fig. 2-1 top**) from three mature individuals of *P. semperi.* Subsequently, the regenerating cerata were collected every day from the animals, which were maintained at 20℃ in aerated sea water under a 10 h light and 14 h dark condition. Since *P. semperi* can receive nutrients from symbiotic dinoflagellates (Kempf 1984; Hoegh-Guldberg et al. 1986; Hoegh-Guldberg and Hinde 1986), we maintained the experimental animals without feeding. For TEM, fully mature cerata longer than 1 mm were excised and collected from an individual of *P. semperi*.

Histological procedures

The animals were anesthetized with 7% $MgCl_2$ solution, dissected in sea water, fixed with Bouin's solution overnight, washed with 70% ethanol, and stored in 70% ethanol at room temperature until use. The tissue samples were dehydrated and cleared through an ethanol-xylene series, embedded in paraffin, and sectioned on a rotary microtome. The serial tissue sections (6 μm thick) were placed on warmed water on glass slides, extended and fixed on the glass slides, dewaxed and hydrated through a xylene-ethanol-water series, and stained with hematoxylin and eosin. Then, the tissue sections were dehydrated and cleared through an ethanol-xylene series, mounted with a coverslip and balsam, and observed under an optical microscope. For TEM, the tissue samples were dissected in 2.5% glutaraldehyde in 0.1 M sodium cacodylate buffer (pH 7.4). The tissues were prefixed in the fixative at 4°C overnight and postfixed in 2% osmium tetroxide for 60 min at 4°C. After dehydration through a water-ethanol series, the tissues were embedded in LR white acrylic resin (Sigma) and sectioned (80

nm thick) on an ultramicrotome. The ultrathin sections were stained with uranyl acetate and lead citrate, and observed under a transmission electron microscope (H-7000; Hitachi).

RESULTS AND DISCUSSION

Fine structure of cnidophages

The fine structures of the cnidosac were observed in detail using TEM. Within the cytoplasm of the cnidophages, multiple nematocysts and numerous vacuolar structures (around 1 μm in diameter) were seen (**Fig. 2-2A**). Magnified images of the cytoplasm revealed several types of vacuoles, granules, and membranous structures, whose nature and functions are elusive. No remarkable structure was found inside the vacuoles of the cnidophages (**Fig. 2-2B**). In the body of cnidarians, the nematocysts are present within the special cells called cnidocytes (Kass-Simon and Scappaticci 2002). In sea slugs that exhibit kleptocnida, however, the cnidocytes are digested but the nematocysts are undigested and incorporated into the cytoplasm of the cnidophages (Kepner 1943). In *P. semperi*. similarly, I observed that naked nematocysts are present within the cytoplasm of the cnidophages (**Fig. 2-2A, C**). Inside the nematocysts, characteristic structures such as barb, thread and capsule (Kass-Simon and Scappaticci 2002) were seen (**Fig. 2-2C**). I found that, notably, numerous granules, 200-400 nm in diameter, membrane-delimited and electron dense, were concentrated around the nematocysts within the cnidophages (**Fig. 2-2B, D**). I suggest the possibility that, although speculative, considering the close association and dense accumulation around the nematocysts, these granules might play some roles in uptake and maintenance of the nematocysts in the cnidophages, although further experimental and functional studies are needed to confirm this idea.

In the cnidophages, no membranous structure, like the endosome formed by phagocytotic incorporation process, was observed around the nematocysts (**Fig. 2-2C, D**), suggesting that the nematocysts may be directly incorporated into the cytoplasm of the cnidophages or the endosomal membrane may be broken after incorporation into the cytoplasm of the cnidophages. A previous study suggested that direct contact of the nematocyst with the cytoplasm of the cnidophage contributes to avoidance of enzymatic digestion by preventing lysosomal fusion (Greenwood and Mariscal 1984). On the other hands, the possibility that the endosomes do exist around the nematocysts but do not fuse to lysosomes has been proposed for some cladobranchian species (Martin 2003). Further studies are

needed to address these unanswered issues.

On ultrastructural implication in functioning of cnidophage

As observed in this study (**Fig. 2-2**), previous TEM studies have reported the presence of intracellular vacuoles in the cnidophages (Greenwood and Mariscal 1984). Meanwhile, to my knowledge, there has been no explicit mentioning on the granules concentrated around the nematocysts that I observed in *P. semperi* (**Fig. 2-2D**). Although the nature and function of the granules are totally unknown, I suggest the possibility that these granules may be lysosome-like orgenelles that are potentially involved in intracellular digestion but unable to digest the nematocysts. The following reports may be somehow relevant to this hypothesis. In a cladobranchian sea slug *Doto acuta* without kleptocnida, it was reported that food-derived nematocysts are carried to the cerata, taken up by the epithelial cells with phagocytic membranes, and digested within the epithelial cells by binding of lysosomes (Martin et. al. 2009). On the other hand, Greenwood and Mariscal (1984) proposed that, in cladobranchian sea slugs with kleptocnida, after the food-derived nematocysts are phagocytosed by the cnidophages, the phagocytic membranes surrounding the nematocysts are broken by some mechanism, by which the nematocysts are freed from digestion by lysosomal fusion.

Some sacoglossan sea slugs are famous for “kleptoplasty”, the phenomenon that the animals incorporate chloroplasts derived from food algae into their digestive tract cells and utilize the plastids for photosynthesis (Rumpho et al. 2000; Rumpho et al. 2011). Upon incorporation into the digestive tract cells, some chloroplasts suffer intracellular digestion whereas other chloroplasts are directly incorporated into the cytoplasm without surrounding vacuolar membranes, thereby escaping lysosome-mediated digestion (Schmitt et al. 2014). In this respect, it is conceivable that kleptocnida and kleptplasty might rely on some common molecular and cellular mechanisms for stable maintenance of heterospecific organelles in molluscan digestive tract cells.

Although several previous studies have argued that the cnidophage may have a receptor-like mechanism for recognizing the nematocysts for taking up a specific nematocyst type (Kepner 1943;

Day and Harris 1978), no concrete evidence has been presented. It is tempting to speculate that the function of the granules densely observed around the nematocysts may be related to such interaction and recognition between the nematocyst and the cnidophage.

Developmental and regeneration processes of cerata

Next, I histologically investigated the formation process of new cerata in detail. By focusing on the tail region and the base of the glove structures, we could sample cerata smaller than 100 μm in size, which are thought to be at early stages of the ceras formation. I observed the developmental process of incipient cerata on the tail (see **Fig. 2-1 bottom**). The sites where the cerata are formed exhibited uplifts with cell proliferation (**Fig. 2-3B**) and that the digestive tract of the trunk extended toward the tip of the cerata (**Fig. 2-3C**). I also observed the developmental process of early cerata at the base of the glove structures (see **Fig. 2-1 bottom**). The thickened epithelial cells, which are presumably differentiating into cnidophages, were identified at the tip of the digestive tract (**Fig. 2-3D**) and a muscle layer surrounding them was formed (**Fig. 2-3E**), which depicted the formation process of a cnidosac. By artificially excising the tip of mature cerata and maintaining the operated animals (see **Fig. 2-1 top**), I sampled the regenerating cerata at different stages and observed the regenerating cnidosacs histologically (**Fig. 2-4**). Just after the ceras tip excision, the structure of the digestive tract around the excised site was unclear, where zooxanthellae and sea slug cells were seen (**Fig. 2-4A-F**). Two or three days after the excision, the wound closed and the digestive tract regenerated toward the tip of the ceras (**Fig. 2-4G, H**). At this stage, no cnidosac-like structure was observed. Four days after the excision, a thick cell aggregation was observed at the tip of the regenerating digestive tract, where active cell proliferation was suggested (**Fig. 2-4I-K**). By the 8th day after the excision, a layer of thick epithelial cells, which are presumably cnidophages-to-be, became evident (**Fig. 2-4L-N**), and 9-13 days after the excision, the epithelial cells became elongated and columnar, where the adjacent cells appeared to adhere to each other and a muscle layer surrounded them (**Fig. 2-4O, P**). By the 27th day after the excision, the presumptive cnidophages further developed and became bell-shaped, with the

muscle layer more developed (**Fig. 2-4Q, R**). Here it should be noted that, because the operated animals were maintained without feeding, these processes of cnidophage formation proceeded without supply and incorporation of cnidarian-derived nematocysts.

Staging of ceras formation

Based on the observations of the developmental and regeneration processes of cerata, I propose the hypothetical developmental scheme of the ceras formation process consisting of five stages (**Fig. 2-5**). At the stage I, an uplift with cell proliferation appears at the site of ceras formation. At the stage II, a ceras process is formed, into which the digestive tract invades. At the stage III, the digestive tract reaches the tip of the ceras, where the epithelial cells proliferate. At the stage IV, the epithelial cells at the tip region, presumptive cnidophages, become tall and attach to each other to form a columnar epithelium, around which a thin muscle layer is formed. At the stage V, the epithelial cells become larger and bell-shaped, forming the shape of a cnidosac surrounded by a muscle layer. According to my observation of the regeneration process (**Fig. 2-4**), the excised cerata reached the stage V around two weeks after the excision (**Fig. 2-4P**), and no new morphological structure was recognized even four weeks after the excision (**Fig. 2-4R**). Therefore, I regarded the stage V cnidosac as structurally in maturity.

It should be noted, however, that there are some potential caveats against the validity of the staging of the cnidosac formation. Firstly, since I have not observed the uptake of nematocysts into the regenerating cnidosacs, whether the stage V cnidosacs are functionally mature or not is to be verified by, for example, experimental feeding of cniderians. Secondly, while the stages I and II were defined mainly based on the observations of the incipient cerata on the tail, the stages III, IV and V were defined mainly based on the observations of the regenerating cerata on the dorsal glove structures (see **Fig. 2-1**). I believe that the scheme summarized in **Fig. 2-5** is basically correct, but the possibility that some missing pieces may exist cannot be ruled out. In this context, accumulation of more developmental and morphogenetic observations on the ceras formation are anticipated.

Phagocytosis and cnidophage

Although not yet verified, the peculiar characteristic of the cnidophage is the capability of incorporating large-sized nematocysts, presumably by phagocytotic activities. In general, the digestive cells of gastropods have sites for receiving food granules at the base of the microvilli by endocytosis (Lobo-da-Cunha et al. 2018), but there has been no report that the normal digestive cells take up nematocyst-sized large particles. Such phagocytosis is also seen in kleptoplastic sea slugs, in which the digestive epithelial cells extend protrusions and take up the chloroplasts (Martin et al. 2013). The process of nematocyst uptake has not been confirmed in the kleptocnida, but it seems plausible that a similar process is operating. Notably, my histological inspection caught a snapshot of pseudopodia-like protrusions extending from newly-formed cnidophages in *P. semperi* (**Fig. 2-6**). The behavior of extended protrusions and taking up of foreign substances is well known in hemocytes. Some mollusks are known to have a peculiar type of hemocytes called amoebocytes, which play a role in cell-mediated immunity (Hildeman 1974). From this point of view, the possibility that the cnidophage may be derived from such hemocytes should be also taken into account, which deserves future studies.

REFERENCES

Day R, Harris L (1978) Selection and turnover of coelenterate nematocysts in some aeolid nudibranchs. Veliger 21: 104–109

Goodheart JA, Bleidißel S, Schillo D, Strong EE, Ayres DL, Preisfeld A, Collins AG, Cummings MP, Wägele H (2018) Comparative morphology and evolution of the cnidosac in Cladobranchia (Gastropoda: Heterobranchia: Nudibranchia). Front Zool 15 43

Greenwood PG, Mariscal RN (1984) The utilization of cnidarian nematocysts by aeolid nudibranchs: Nematocyst maintenance and release in *Spurilla*. Tissue Cell 16: 719–730

Hildeman WH (1974) Phylogeny of immune responsiveness in invertebrates. Life Sci 14: 605–614

Hoegh-Guldberg O, Hinde R (1986) Studies on a nudibranch that contains zooxanthellae. I. Photosynthesis, respiration and the translocation of newly fixed carbon by zooxanthellae in Pteraeolidia ianthina. Proc R Soc Lond B 228: 493-509

Hoegh-Guldberg O, Hinde R, Muscatine L, Smith DC (1986) Studies on a nudibranch that contains zooxanthellae. II. Contribution of zooxanthellae to animal respiration (CZAR) in Pteraeolidia ianthina with high and low densities of zooxanthellae. Proc R Soc Lond B 228(1253): 511-521

Kass-Simon G, Scappaticci AA (2002) The behavioral and developmental physiology of nematocysts. Can J Zool 80: 1772-1794

Kempf SC (1984) Symbiosis between the zooxanthella Symbiodinium (= Gymnodinium) microadriaticum (Freudenthal) and four species of nudibranchs. Biol Bull 166: 110-126

Kepner WA (1943) The manipulation of the nematocysts of *Pennaria tiarella* by *Aeolis pilata*. J Morphol 73: 297–311

Lobo-da-Cunha A, Alves Â, Oliveira E, Guimarães F, Calado G (2018) Endocytosis, lysosomes, calcium storage and other features of digestive-gland cells in cephalaspidean gastropods (Euopisthobranchia). J Molluscan Stud 84: 451-462

Martin R (2003) Management of nematocysts in the alimentary tract and in cnidosacs of the aeolid nudibranch gastropod *Cratena peregrina*. Mar Biol 143: 533–541

Martin R, Heß M, Schrödl M, Tomaschko KH (2009) Cnidosac morphology in dendronotacean and aeolidacean nudibranch molluscs: from expulsion of nematocysts to use in defense? Mar Biol 156: 261–268

Martin R, Walther P, Tomaschko KH (2013) Phagocytosis of algal chloroplasts by digestive gland cells in the photosynthesis-capable slug *Elysia timida* (Mollusca, Opisthobranchia, Sacoglossa). Zoomorphology 132: 253–259

Miller JA, Byrne M (2005) Ceratal autotomy and regeneration in the aeolid nudibranch *Phidiana crassicornis* and the role of predators. Invertebr Biol 119: 167–176

Rubin DI, Bode HR (1982) Nematocyte development in Hydra attenuata is dependent on both the interstitial cells and the epithelial cells. Dev Biol 90: 306–314

Rumpho M E, Pelletreau KN, Moustafa A, Bhattacharya D (2011) The making of a photosynthetic animal. J Exp Biol 214(2): 303-311

Rumpho ME, Summer EJ, Manhart JR (2000) Solar-powered sea slugs. Mollusc/algal chloroplast symbiosis. Plant Physiol 123: 29–38

Schmitt V, Händeler K, Gunkel S, Escande ML, Menzel D, Gould SB, Martin WF, Wägele H (2014) Chloroplast incorporation and long-term photosynthetic performance through the life cycle in laboratory cultures of *Elysia timida* (Sacoglossa, Heterobranchia). Front Zool 11 5

Voltzow J (1994) Gastropoda: Prosobranchia. In: Harrison FW, Kohn AJ (eds) New York: Wiley-Liss Inc

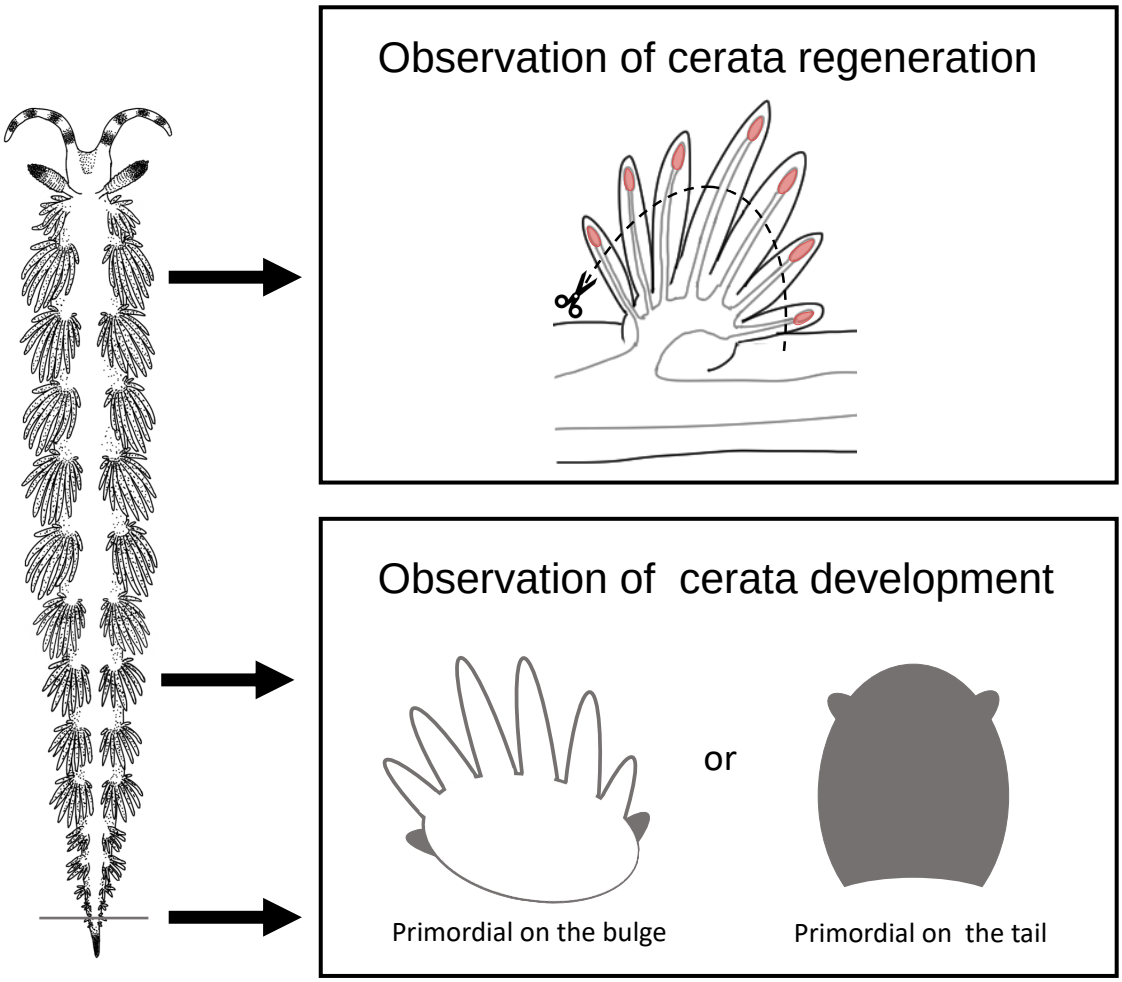

Fig. 2-1. The scheme of observation of development and regeneration of cerata of *P. semperi*.

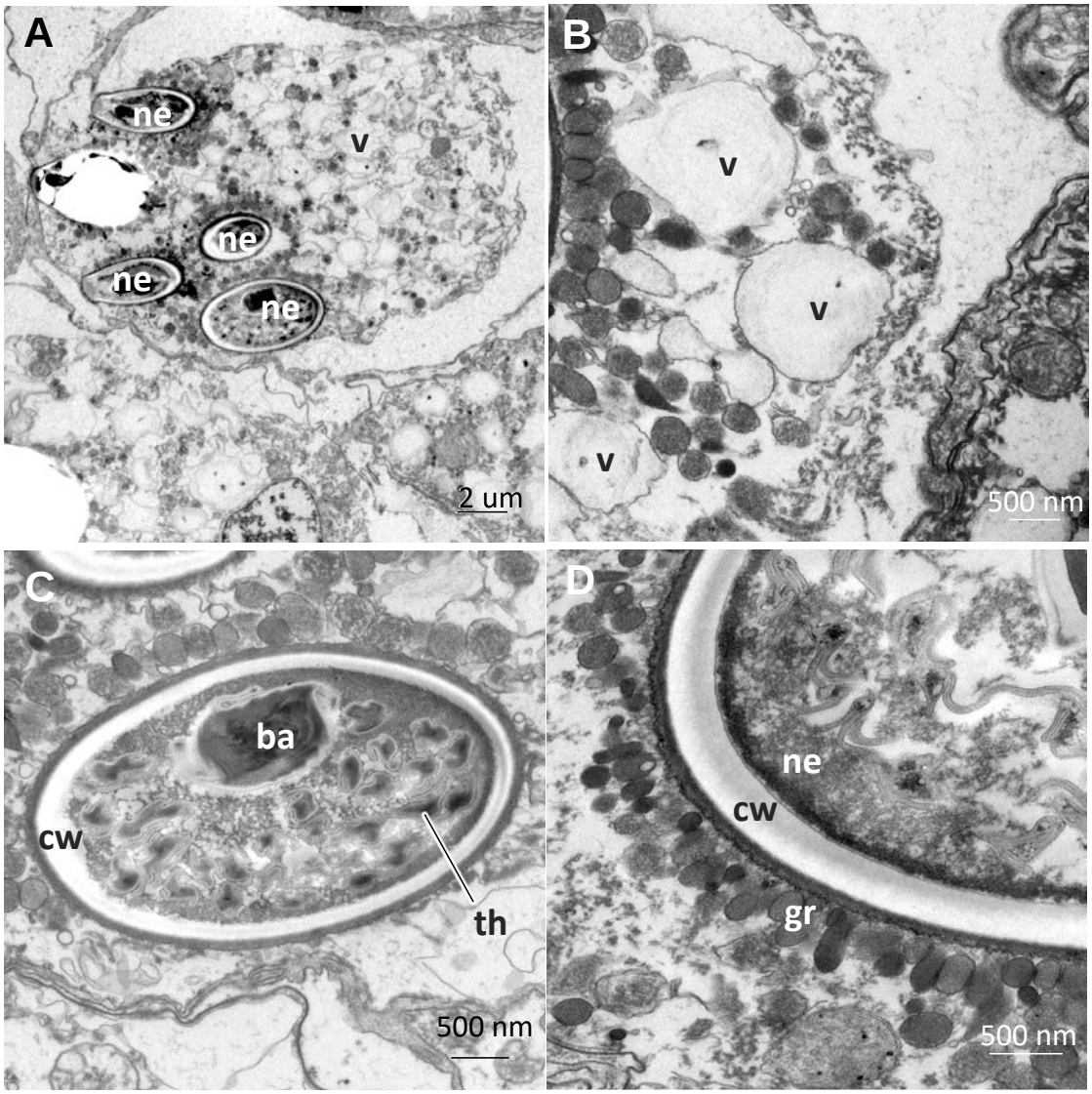

Fig. 2-2. TEM images of cnidophage of *P. semperi.* (A) A cnidophage, in which four nematocysts (ne) and a number of vacuoles (v) are seen. (B) A magnified image of the vacuoles (v). (C) A nematocyst in the cytoplasm of the cnidophage. The cross section of barb (ba) and thread are seen inside of capsule wall. (D) A magnified image of the intracellular nematocyst, around which numerous granular structures (gr) are seen. Abbreviations: ne, nematocyst; v, vacuole; ba, barb; th, thread; cw, capsule wall; gr, granular structure.

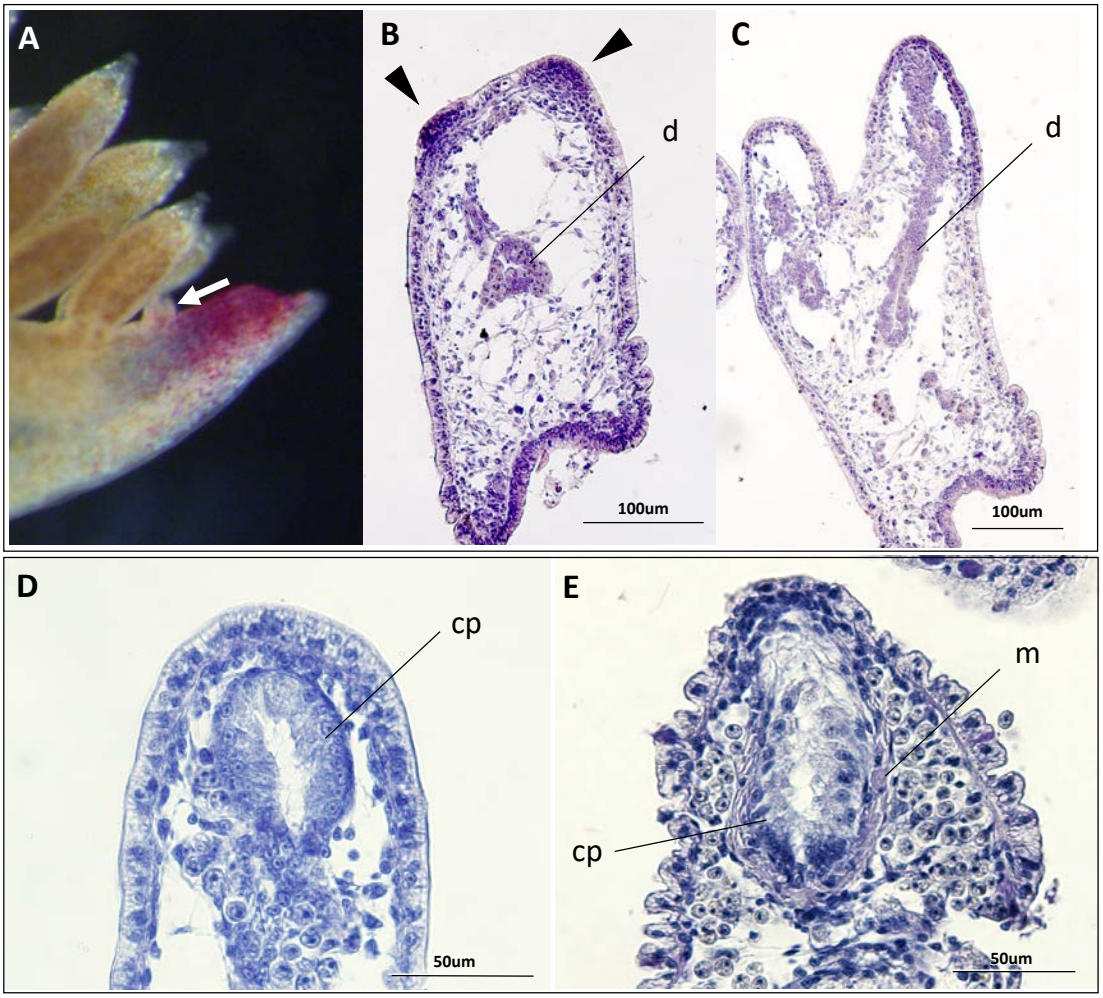

Fig. 2-3. Formation process of new cerata of *P. semperi*. (A) A primordial ceras on the tail (arrow). (B, C) Tissue images of incipient cerata on the tail smaller than 100 μm long. Arrowheads indicate the uplifts with cell proliferation. (D, E) Tissue images of immature cerata on the base of glove structures around 100-300 μm long. Abbreviations: cp, cnidophage; d, digestive tract; m, muscle layer.

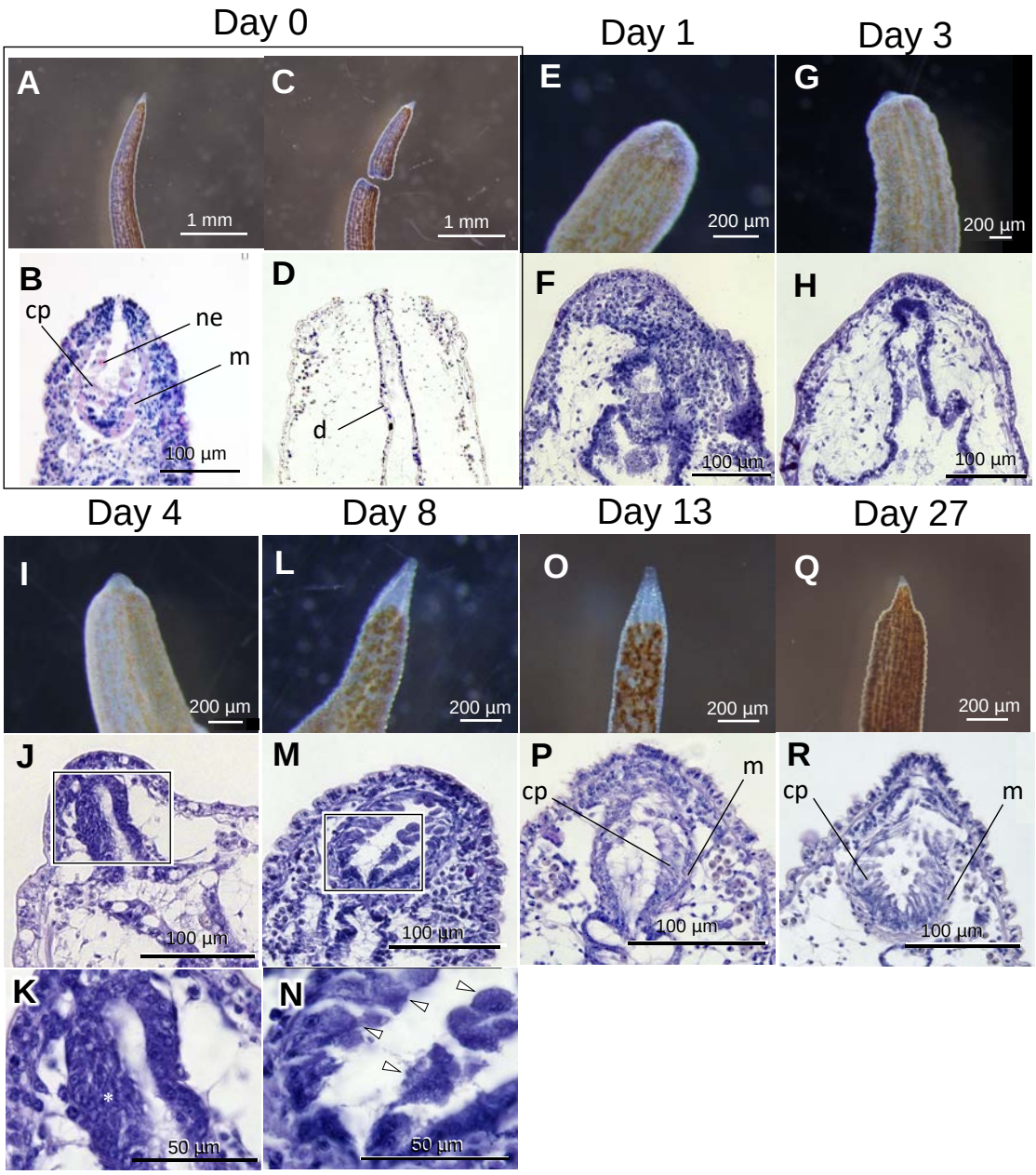

Fig. 2-4. Regeneration process of cerata after experimental excision of the tip in *P. semperi*. (A, B) Intact ceras tip before excision. (C, D) Ceras tip just after excision. (E, F) Ceras tip 1 day after excision. (G, H) Ceras tip 3 days after excision. (I, J, K) Ceras tip 4 days after excision. (L, M, N) Ceras tip 8 days after excision. (O, P) Ceras tip 13 days after excision. (Q, R) Ceras tip 27 days after excision. Abbreviations: cp, cnidophage; d, digestive tract; m, muscle layer; ne, nematocyst.

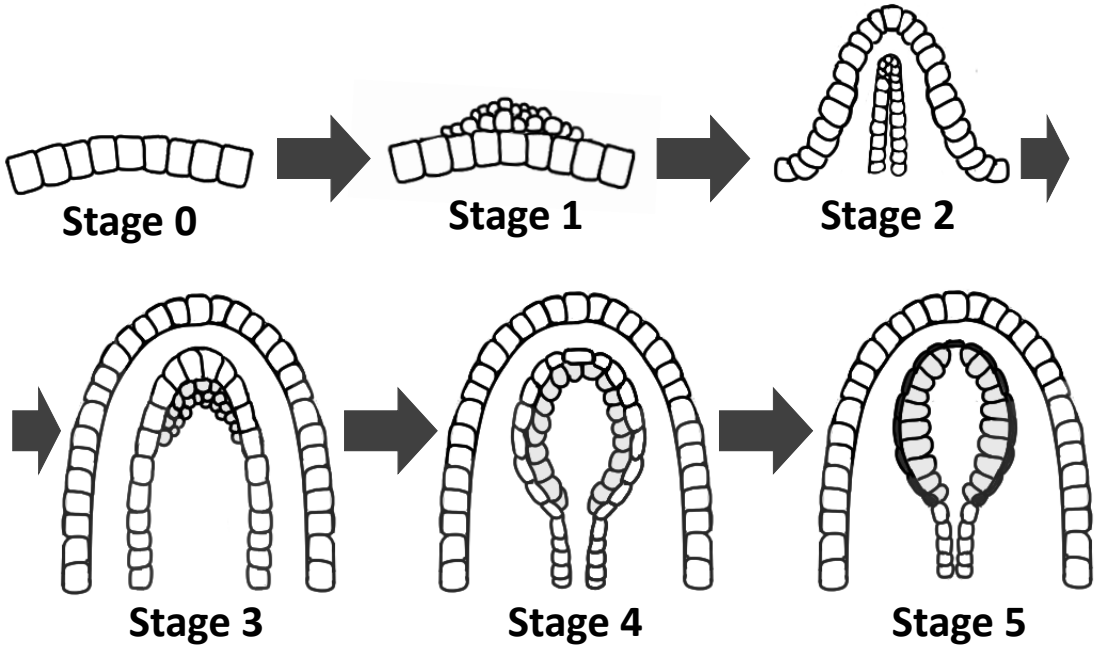

Fig. 2-5. The hypothetical developmental scheme of the ceras formation process consisting of five stages.

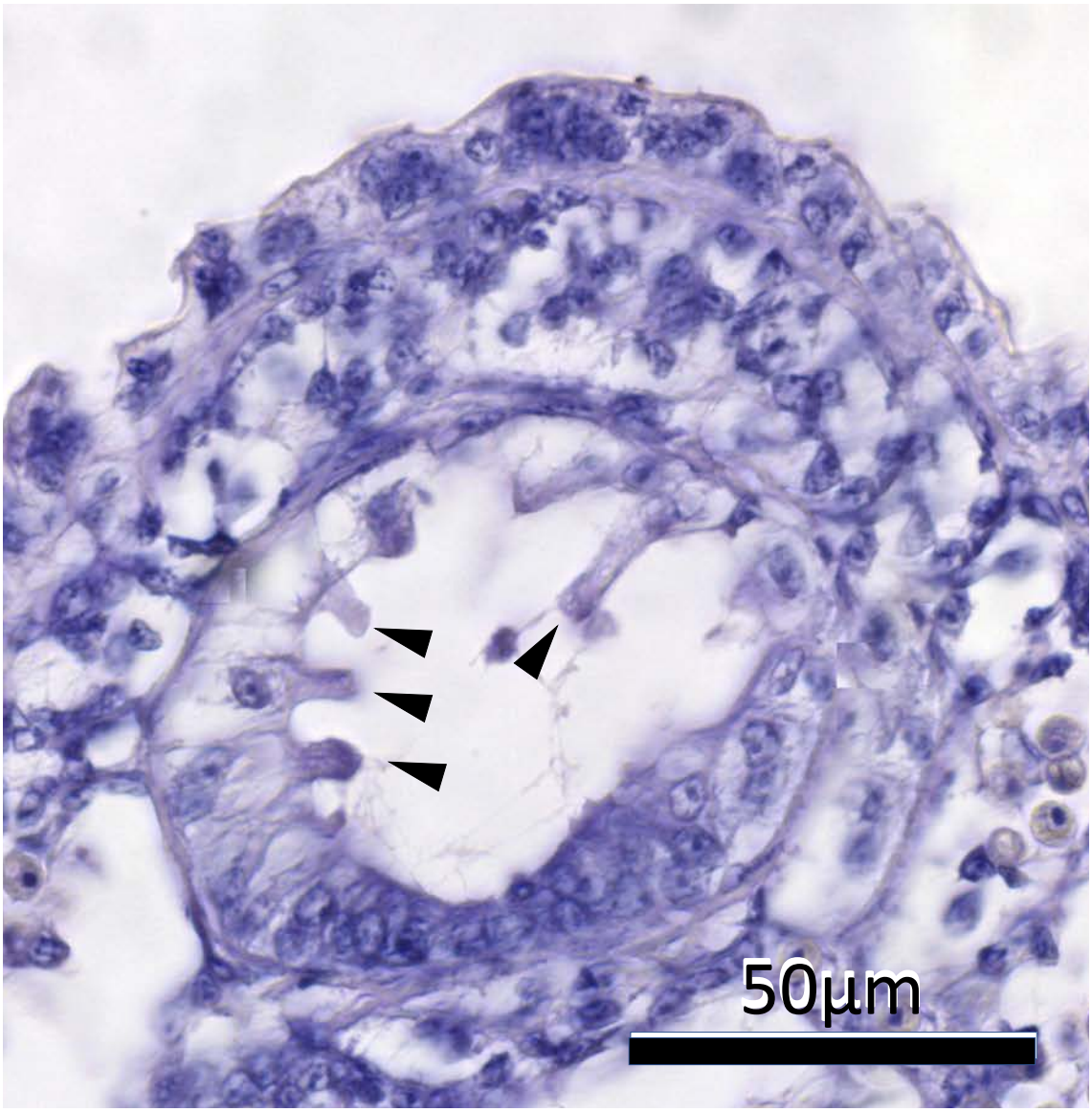

Fig. 2-6. A regenerating cnidosac 13 days after the excision, in which the newly-formed cnidophages extend pseudopodia-like projections on the apical side (arrowheads).

Part Ⅲ

Transcriptomics and proteomics of cnidosac: insight into molecular mechanisms underpinning kleptocnida in *Pteraeolidia semperi*

INTRODUCTION

Kleptocnida, or nematocyst stealing, found in some cladobranchian sea slugs is a very unique phenomenon in that intracellular organelles of cnidarians called nematocysts are incorporated into molluscan gut epithelial cells, which might represent an initial stage of establishing a novel endosymbiotic association between totally different organisms (Grosvenor 1903; Edmunds 1966; Greenwood and mariscal 1984).

In this context, kleptoplasty, or plastid stealing, known from some sacoglossan sea slugs, is a totally different but conceptually analogous phenomenon, in which chloroplasts of food algae are incorporated into the molluscan digestive organ and function there, by which nutrients are produced for the animals by photosynthesis using the algal chloroplasts (Hoegh-Guldberg et al. 1986; Hoegh-Guldberg and Hinde 1986). Laboratory culturing methods were established for several species of kleptoplastic sea slugs (Pelletreau et al. 2012; Schmitt et al. 2014), by which chloroplast-free juvenile animals can be produced and used for experimental works. For example, the gene expression dynamics were investigated during the acquisition process of alga-derived chloroplasts in a kleptoplastic sea slug *Elysia chlorotica* (Chan et al. 2018). However, the mechanisms by which chloroplasts are taken up and maintained in the host cells have been totally unknown in the kleptoplastic sea slugs.

Thus far, no molecular genetic studies have been conducted on cladobranchian sea slugs with kleptocnida, mainly because of the difficulty in culturing and maintaining them in laboratory for an extended period. However, recent development of transcriptomic, proteomic and metabolomic technologies have made it possible to analyze genes and proteins of field-collected biological samples that are often very small in quantity. In Part I and Part II of this thesis, I described the structure, localization, morphogenesis and development of the ceras, the cnidosac and the cnidophage, the organ,

the tissue and the cell for kleptocnida in *P. semperi*. Considering that cnidarian-derived stolen nematocysts are localized to the cnidophage, the cnidosac and/or the cnidophage should be the targets to understand the molecular and cellular mechanisms of kleptocnida.

In this study, in order to understand the molecular aspects of kleptocnida, I performed transcriptomic analysis of the kleptocnida-related tissue samples, namely the excised ceras tips, in comparison with the other tissue samples such as the excised ceras bases, the head tentacles and the oral tentacles, by which I attempted to identify the genes highly and specifically expressed in the cnidosacs. I also performed proteomic analysis of the dissected cnidosacs and the secretion samples squeezed from the ceras tips, by which I attempted to identify the proteins abundant in the cnidosacs. Based on these cnidosac-related molecular data, I argue and speculate how these molecules are potentially involved in kleptocnida.

MATERIALS AND METHODS

Sample preparation, RNA extraction, and library construction

The samples of *P. semperi* were collected from a shore reef of Araihama, Miura City, Kanagawa Prefecture, Japan. The collected animals were maintained in a sea water tank at 20°C under a 10 h light and 14 h dark condition without feeding. RNA was extracted from the following body parts or samples of *P. semperi*: oral tentacles, head tentacles, tips of cerata, bases of cerata, isolated cnidosacs, and secretion squeezed from cnidosacs (**Fig. 3-1**). For RNA extraction, large cerata of 1 mm or longer in size were used, from which the middle part was discarded upon dissection of the tip and basal parts. For cnidosac isolation, the cerata were immersed in 99.5% ethanol for 1 min, transferred to PBS and dissected with fine tweezers. For sampling mucus from cnidosacs, the cerata were placed in PBS and squeezed with fine tweezers, by which the mucus extruded from the tip of the cerata was collected by a micropipette.

Each sample was placed in 0.5-1.0 ml of ISOGENE (NIPPON GENE Co. Ltd., Tokyo, JP), homogenized, vigorously mixed with 200 µl of chloroform for 15 sec, and centrifuged at 12,000 rpm for 15 min at 4°C. The aqueous layer was transferred to a new tube and mixed with 500 µl of isopropanol, and the mixture was placed for 10 min at room temperature and centrifuged at 12,000 rpm for 10 min at 4°C. The supernatant was discarded, and the precipitated RNA was washed with 1 ml of 70% ethanol, dried for 5 min, and dissolved in 40 µl nuclease-free water. The RNA samples were prepared in triplicate, and purified with RNAClean XP (Beckman Coulter Life Sciences Japan, Tokyo, JP).

The TruSeq RNA Sample Prep Kit (Illumina, Inc, Tokyo, JP) was used for library preparation from the RNA samples of the mouth tentacles, the head tentacles, and the tips of cerata and the bases of cerata. Since the RNA samples extracted from the isolated cnidosacs and the secretion squeezed from the cnidosacs were very small in amount, the Nextera XT DNA Library Preparation Kit (Illumina, Inc, Tokyo, JP) and SMART-Seq v4 Ultra Low Input RNA Kit for Sequencing (Takara Bio Inc., Shiga , JP) were used for library preparation.

RNA-seq, sequence assembly and Blast search

The quality of raw RNA-seq data was checked by using FastQC (http://www.bioinformatics.babraham.ac.uk/projects/fastqc/), and adapter sequences and low-quality reads were eliminated by using Trimomatic (Bolger et al. 2014). Subsequently, de novo assembly was performed using Trinity (Grabherr et al. 2011), and transcript quantification was carried out by Salmon (Patro et al. 2017). Blast X homology searches were performed against the Swiss-Prot database and the datasets of mollusks (*Pomacea canaliculata, Lottia gigantea, Crassostrea gigas, Crassostrea virginica, Octopus bimaculoides, Octopus vulgaris, Mizuhopecten yessoensis* and *Pecten maximus*), cnidarians (*Hydra vulgaris, Nematostella vectensis,* and *Stylophora pistillata*) and the dinoflagellate *Symbiodinium microadriaticum* protein sequences registered in the NCBI database. Gene functions were also inferred from the result of Trinotate (Bryant et al. 2017). Clustering analysis of the transcriptional profiles was performed using the hclust command in R.

Detection of differentially expressed genes

The gene expression levels were shown in terms of transcripts per million (TPM) values. A gene was regarded as highly and specifically expressed at the tip of cerata when either of the following criteria was fulfilled: (i) given that the TPM value at the tip of cerata is larger than 100, the value is more than twice higher than the TPM values at the base of cerata, the head tentacles and the oral tentacles; (ii) given that the TPM value at the tip of cerata is between 10 and 100, the value is more than five times higher than the TPM values at the base of cerata, the head tentacles and the oral tentacles.

Protein extraction

The samples of the isolated cnidosacs and the secretion squeezed from the cnidosacs were subjected to protein extraction. For isolation of the cnidosacs, the cerata were immersed in 99.5% ethanol for 1 min, transferred to PBS, and dissected with fine tweezers. For sampling of the secretion, the cerata

were placed in PBS and squeezed with fine tweezers, by which the mucus extruded from the tip of the cerata was collected by a micropipette. Then each sample was homogenized in 50 µl of 50 mM HCl (pH 7.5). The isolated cnidosac sample was mixed with 60 µl SDS buffer and 5.5 µl of 2-mercaptoethanol, heat-treated at 99°C for 5 min, and then centrifuged at 15,000 x g for 10 min to collect the supernatant. To retrieve proteins, 60 µl of chloroform and 180 µl of ethanol were mixed with the supernatant, and then 180 µl of distilled water was added, vortexed, and centrifuged at 15,000 x g for 10 min. After the upper aqueous layer was discarded, 200 µl of methanol was added. The mixture was centrifuged at 15,000 x g for 10 min to precipitate proteins. The supernatant was discarded and the precipitate was dried. For the secretion sample, 200 µl of 10% trichloroacetic acid in acetone was added, and the mixture was incubated overnight at –20°C. After centrifugation at 12,000 x g for 10 min, the supernatant was discarded. The protein pellet was rinsed with 500 µl of acetone, and dried until acetone was completely evaporated. These dried samples were stored in a refrigerator at –80°C until use.

Shotgun proteomics

The protein samples were resuspended to 50-100 µl of PTS solution (Phase-Transfer-Surfactant ; 12 mM sodium deoxycholate, 12 mM sodium lauroylsarcosinate, 100 mM Tris-HCl (pH 9.0)), and heated at 95°C for 5 min. Then, 500 mM dithiothreitol solution was added to make a final concentration at 20 mM, and incubated at 95°C for 10 min. Furthermore, 500 mM iodoacetoamide solution was added to make the final concentration at 40 mM, and the mixture was placed in the dark at room temperature for 60 min. For enzymatic digestion, 200 ng of Trypsin/Lys-C Mix (Promega Co., Tokyo, JP) in 50 mM ammonium hydrogen carbonate solution was added and incubated at 37°C for 16 h. To remove surfactants, the same amount of ethyl acetate was added to the sample solution, and 0.5% volume of trifluoroacetic acid was added and mixed vigorously. The mixture was centrifuged at 15,000 x g, 25°C for 2 min, and the upper layer (the ethyl acetate layer) was removed with a pipette. The remnant solution was dried in vacuo, and resuspended to 100 µl 5% acetonitrile and 1% formic acid containing

water for further purification using GL-Tip SDB (GL Science, Tokyo, JP). The peptides eluted from GL-Tip SDB were subjected to LC-MS analysis using ACQUITY UPLC H-Class (Waters. Tokyo, JP) and Xevo G2-XS QToF (Waters, Tokyo, JP). Peptide separation was performed using a CSH column (2 mm id, 150 mm, Waters, Tokyo, JP), and their mass data were obtained using a MS^E (positive) mode. Protein identification was performed using ProteinLynx Global Server (Waters, Tokyo, JP) by reference to the protein sequences deduced from the transcriptome analysis.

RESULTS AND DISCUSSION

Transcriptome analysis

RNA-seq reads from the oral tentacles, the head tentacles, the tips of the cerata and the bases of the cerata were assembled into 89,726 contigs in total. On the other hand, RNA-seq reads from the isolated cnidosacs and the secretion from squeezed from the cnidosacs were, because of the low RNA titers, too small in number to construct reliable contigs by de novo assembly, so they were not used for further analysis. Of 89,726 contigs, 165 were identified as specifically highly expressed at the tip of the cerata (**Table 3-1; Fig. 3-2)**. Clustering analysis of the RNA-seq data confirmed the organ-specific gene expression patterns in which the tips and the bases of the cerata clustered and the head and oral tentacles are intermingled (**Fig. 3-3**). The top-ranked highly expressed genes contained myosin, calmodulin, phospholipase, zinc metalloproteinase, sodium-dependent phosphate transport, arginase 1, cyclophilin type peptidyl-prolyl cis-trans isomerase/CLD, conopressin/neurophysin, NIPSNAP homolog, and genes encoding mannose receptor protein with C-type lectin domain, ShK domain, and C1q domain. In addition, many genes whose function is unknown were also identified.

Proteome analysis

The numbers of proteins identified from the cnidosac samples and the secretion samples were 388 and 189, respectively (**Fig. 3-4**). The top 50 proteins identified from the cnidosac samples are listed (**Table 3-2**), which were dominated by muscle- and cytoskeleton-related proteins such as myosin, tubulin, actin and others. Several proteins that make up collagens were also ranked in the list. A mannose receptor protein with c-type lectin domain and an endocysosis-related protein were also identified in the cnidosac samples. The top 50 proteins identified from the secretion samples are also listed (**Table 3-3**), in which muscle- and cytoskeleton-related proteins were also identified but collagen-related proteins were not. In addition, a hydrolase phospholipase A2 and a phagocytosis related protein ranked in the list.

On muscle-, cytoskeleton- and collagen-related proteins identified from cnidosac

The transcriptome analysis revealed that the majority of highly-expressed transcripts in the tip of cerata are such genes as actin, myosin, tubulin, calmodulin, Zinc metalloproteinase, etc., which are related to muscle or cytoskeleton (**Table 3-1**). The proteome analysis also identified a number of muscle- and cytoskeleton-related proteins in the cnidosac samples (**Table 3-2; Table 3-3**). Several collagen proteins are identified among the cnidosac proteins (**Table 3-2**). These proteins are probably attributed to the well-defined muscle layer surrounding the cnidosac (see **Fig. 2-3; Fig. 2-4**). The cnidophages that actively form pseudopodia-like projections (see **Fig. 2-6**) may also contribute to the cytoskeletal proteins.

Presumable functions of transcripts and proteins expressed in cnidosac

In both the transcriptome and the proteome, several proteins with a C-type lectin domain were identified as highly expressed in the cnidosac samples. C-type lectins are sugar chain-binding proteins with a conservative sugar chain recognition domain, which are known to bind to various ligands other than sugar chains (Kerrigan and Brown 2009). The C-type lectin superfamily is a large group of proteins characterized by the presence of one or more C-type lectin-like domains (Drickamer and Fadden 2002). It has been reported that some C-type lectins are involved in uptake of substances via phagocytosis, and macrophages express various lectin receptors on their cell surface to recognize pathogens (Stahl 1992). Among C-type lectins, the mannose receptor identified in this study is known to contribute to cell adhesion and other cellular functions, but it is elusive whether it plays a role in phagocytosis (Kim 2012).

Proteins with the C1q domain were also identified as highly expressed in both the transcriptome and the proteome of the cnidosac samples. The C1q protein plays an important role in the complement reaction of vertebrates by specifically binding to pathogens and opsonizing them (Bohlson et al. 2007; Ghai et al. 2007). The establishment of the complement system is evolutionarily older than the adaptive immune system, and vertebrates, invertebrates, and

prokaryotes also carry proteins evolutionarily related to the complement system (Carland and Gerwick 2010). There are multiple homologues of C1q domain proteins such as C1q-like proteins, C1q, ghC1q, sghC1q and cgHC1q proteins, which are considered to be functionally diversified in the immune response system (Ghai et al. 2007), but detailed studies have been scarce. A previous study suggested that a protein with a C1q domain in a scallop species may contribute to pathogen binding in the immune system (Wang et al. 2012).

Ras-related proteins Rab7a and Rab35 were identified in the proteome of the cnidosac samples. These proteins were reported to be endocytosis-related, which may be involved in endosome maturation and actin-dependent phagosome formation, respectively (Choi 2018; Egami et al. 2011).

These transcriptomic and proteomic results taken together, I point out that multiple proteins related to binding and phagocytotic uptake of microbes and other foreign substances are expressed at the tip of cerata of *P. semperi*. It seems plausible, although speculative, that these molecules may be involved in recognition and incorporation of the nematocysts by the cnidophages. The observation that the cnidophages sometimes exhibit pseudopodia-like projections, which is indicative of phagocytotic activity (see **Fig. 2-6**), may be in favor of this hypothesis. In order to confirm this idea, further studies on localization and function of these proteins, by employing in situ hybridization, immunohistochemistry and RNA interference, are needed.

REFERENCES

Bohlson SS, Fraser DA, Tenner AJ (2007) Complement proteins C1q and MBL are pattern recognition molecules that signal immediate and long-term protective immune functions. Mol Immunol 44: 33–43

Bolger AM, Lohse M, Usadel B (2014) Trimmomatic: a flexible trimmer for Illumina sequence data. Bioinformatics 30: 2114–2120

Bryant DM, Johnson K, DiTommaso T, Tickle T, Couger MB, Payzin-Dogru D, Lee TJ, Leigh ND, Kuo TH, Davis FG, Joel B, Sevara B, Anna RG, Stephanie LT, Steven C, William WY, Robert MF, Leonid P, Clifford JT, Aviv R, Brian JH, Jessica LW (2017) A tissue-mapped axolotl de novo transcriptome enables identification of limb regeneration factors. Cell Rep 18: 762–776

Carland TM, Gerwick L (2010) The C1q domain containing proteins: Where do they come from and what do they do? Dev Comp Immunol 34: 785–790

Chan CX, Vaysberg P, Price DC, Pelletreau KN, Rumpho ME, Bhattacharya D (2018) Active Host Response to Algal Symbionts in the Sea Slug Elysia chlorotica. Mol Biol Evol 35: 1706–1711

Edmunds M (1966) Protective mechanisms in the Eolidacea (Mollusca Nudibranchia). J Lin Soc Lond Zool 46: 27–71

Ghai, R, Waters P, Roumenina LT, Gadjeva M, Kojouharova MS, Reid KBM, Sim RB, Kishore U (2007) C1q and its growing family. Immunobiology 212: 253–266

Greenwood PG, Mariscal RN (1984) The utilization of cnidarian nematocysts by aeolid nudibranchs: Nematocyst maintenance and release in *Spurilla*. Tissue Cell 16: 719–730

Grosvenor G (1903) On the nematocysts of aeolids. Proc R Soc Lond 72: 462–486

Choi S ed (2018) Ras-Related Protein Rab-7a. In Encyclopedia of Signaling Molecules (Cham: Springer International Publishing), 4501–4501

Drickamer K, Fadden AJ (2002) Genomic analysis of C-type lectins. Biochemical Society Symposia 69: 59–72

Egami Y, Fukuda M, Araki N (2011) Rab35 regulates phagosome formation through recruitment of ACAP2 in macrophages during Fc R-mediated phagocytosis. J Cell Sci 124: 3557–3567

Ghai R, Waters P, Roumenina LT, Gadjeva M, Kojouharova MS, Reid KBM, Sim RB, Kishore U (2007). C1q and its growing family. Immunobiology 212: 253–266

Grabherr MG, Haas BJ, Yassour M, Levin JZ, Thompson DA, Amit I, Adiconis X, Fan L, Raychowdhury R, Zeng Q, Chen Z, Mauceli E, Hacohen N, Gnirke A, Rhind N, di Palma F, Birren BW, Nusbaum C, Lindblad-Toh K, Friedman N, Regev A (2011) Full-length transcriptome assembly from RNA-Seq data without a reference genome. Nat Biotechnol 29: 644–652

Kerrigan AM, Brown GD (2009) C-type lectins and phagocytosis. Immunobiology 214 562–575

Kim JH (2012) Functional roles of mannose-binding protein in the adhesion, cytotoxicity and phagocytosis of Acanthamoeba castellanii. Exp Parasitol 132: 287–292

Pelletreau KN, Worful JM, Sarver KE, Rumpho ME (2012) Laboratory culturing of Elysia chlorotica reveals a shift from transient to permanent kleptoplasty. Symbiosis 58: 221-232

Patro R, Duggal G, Love MI, Irizarry RA, Kingsford C (2017) Salmon provides fast and bias-aware quantification of transcript expression. Nat Methods 14: 417–419

Schmitt V, Händeler K, Gunkel S, Escande ML, Menzel D, Gould SB, Martin WF, Wägele H (2014) Chloroplast incorporation and long-term photosynthetic performance through the life cycle in laboratory cultures of *Elysia timida* (Sacoglossa, Heterobranchia). Front Zool 11: 5

Wang L, Wang L, Zhang H, Zhou Z, Siva VS, Song L (2012) A C1q domain containing protein from scallop *Chlamys farreri* serving as pattern recognition receptor with heat-aggregated IgG binding activity. PLoS One 7: e43289

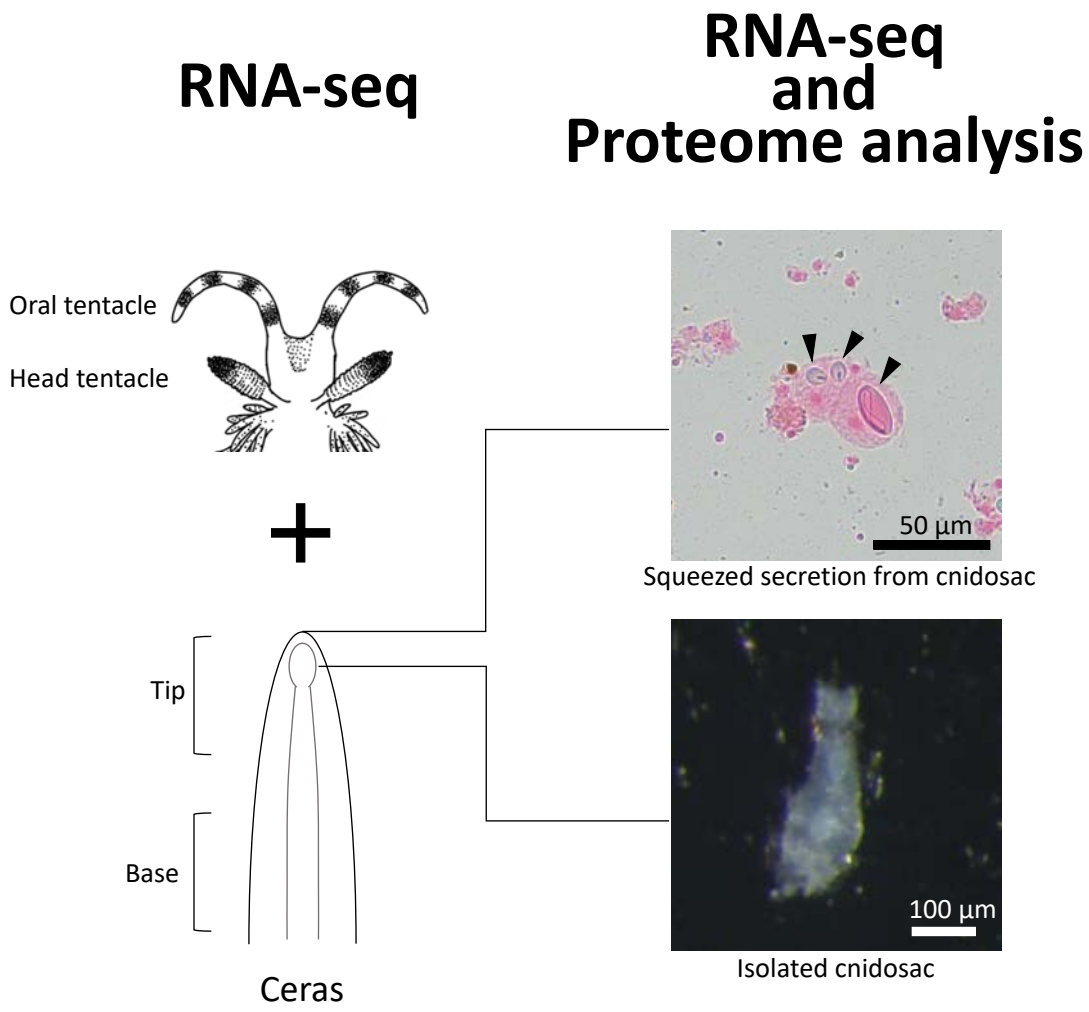

Fig. 3-1. The experimental scheme of RNA-seq and mass spectrometry for the transcriptomic and proteomic analyses of the tip of cerata and other body parts of *P. semperi*.

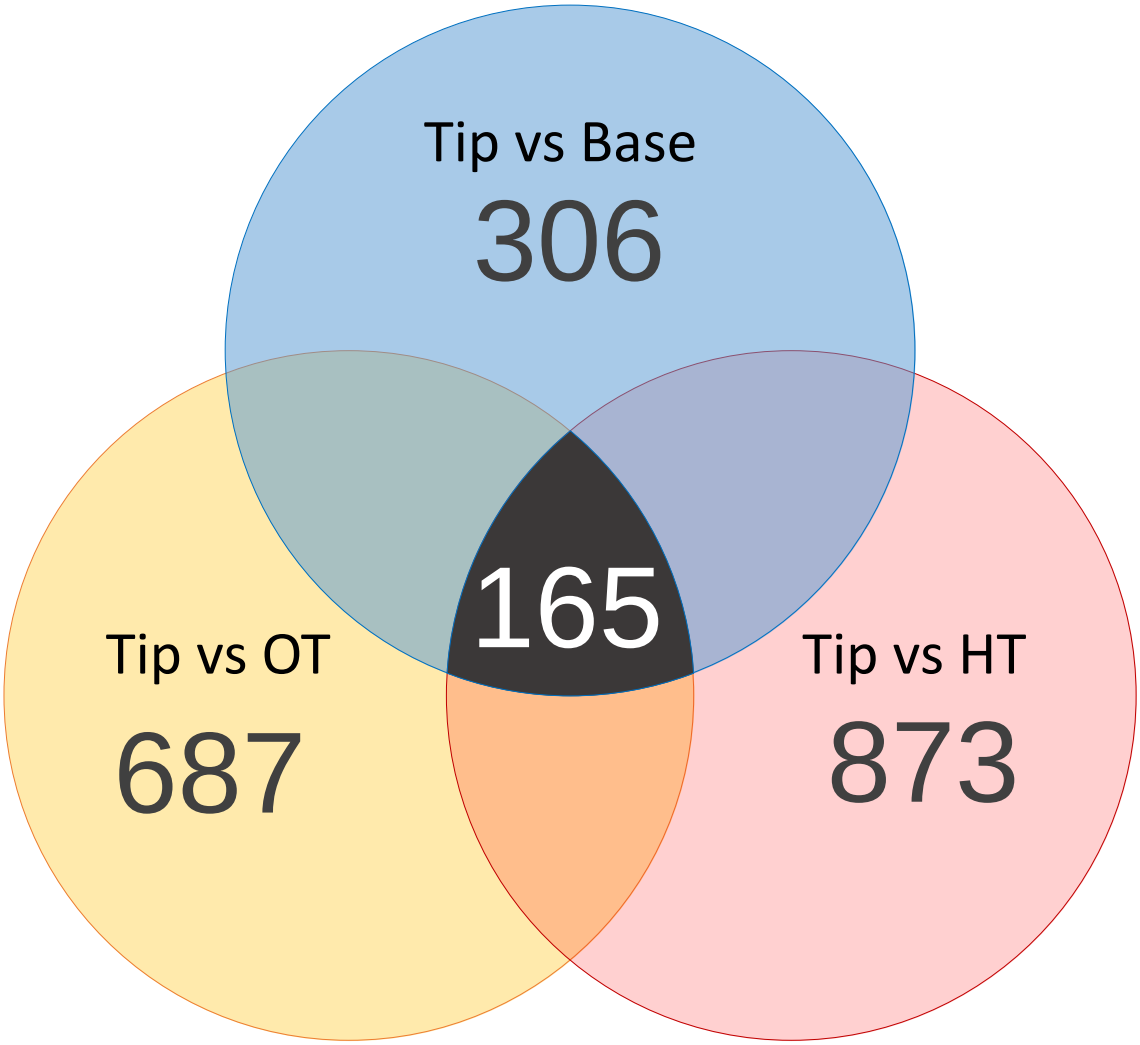

Fig. 3-2. Venn diagram showing the number of transcripts highly and specifically expressed in the tip of cerata in comparison with the other tissues of *P. semperi*. OT and HT means oral tentacles and head tentacles, respectively.

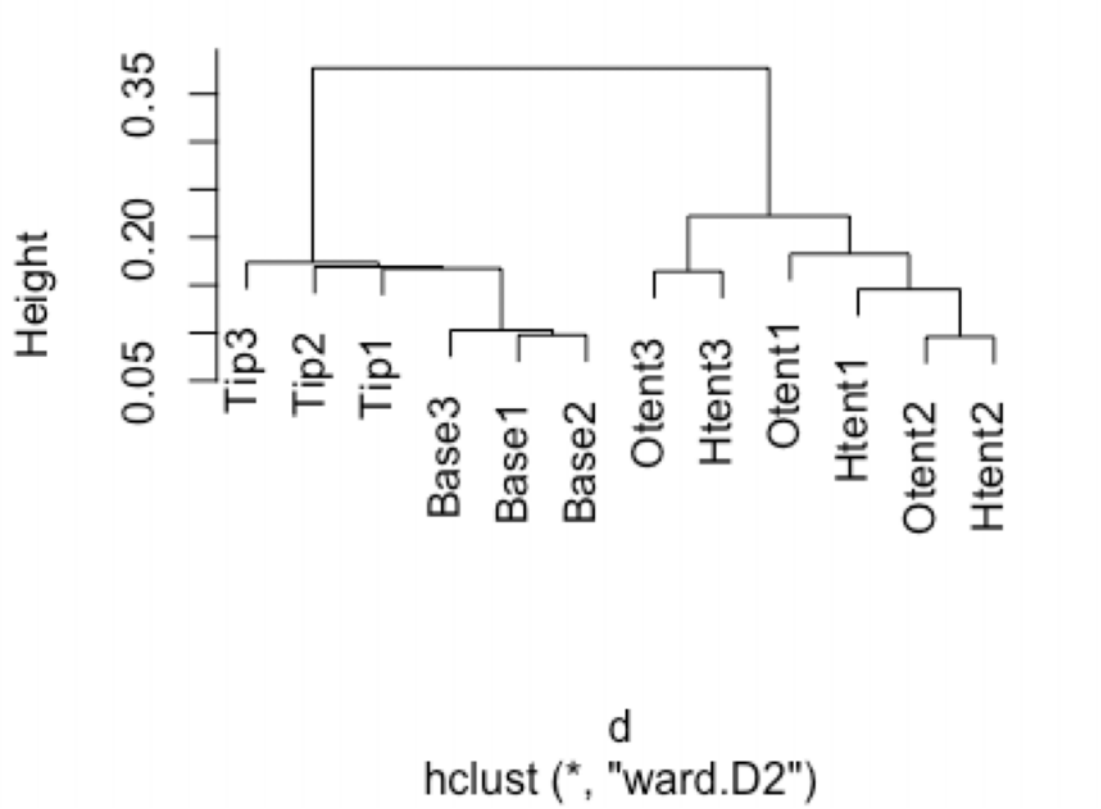

Fig. 3-3. Clustering analysis of gene expression patterns based on RNA-seq data of the dissected tissues of *P. semperi*. Tip, tip of cerata; Base, base of cerata; Htent, head tentacles; Otent, oral tentacles (see **Fig. 12**).

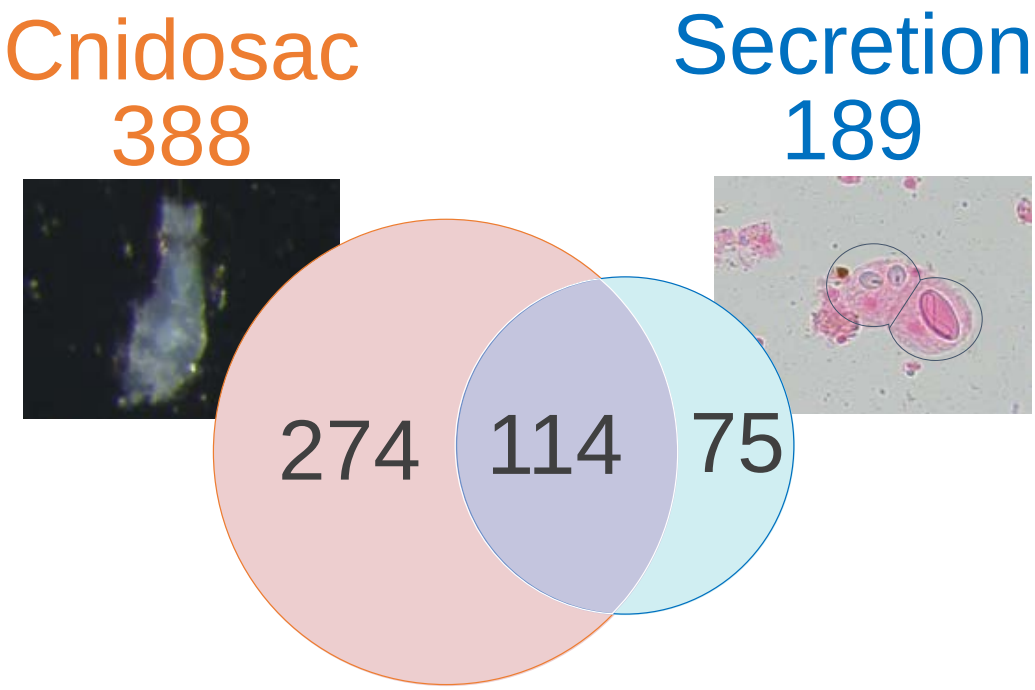

Fig. 3-4. Venn diagram showing the number of proteins identified from the isolated cnidosacs and the the secretion samples from cerata of *P. semperi*.

Table 3-1. The top 50 list of transcripts highly and specifically expressed in the tip of cerata of *P. semperi* , arranged in the order of expression level (TPM).

Rank	Name	TPM	Annotation	e-value
1	DN24725_c0_g1_i6	4865.9	-	-
2	DN24725_c0_g1_i2	4018.7	-	-
3	DN9823_c0_g2_i1	2446.5	-	-
4	DN82606_c0_g1_i1	2125.3	-	-
5	DN12502_c0_g1_i1	1858.4	myosin_essential_light_chain	8.57E-79
6	DN994_c0_g1_i1	1402.0	-	-
7	DN44929_c0_g1_i1	1370.5	-	-
8	DN33854_c0_g1_i1	1310.5	-	-
9	DN21713_c0_g1_i1	1214.3	-	-
10	DN9823_c0_g1_i2	1171.9	-	-
11	DN85806_c0_g1_i1	1092.6	phospholipase A2	2.00E-20
12	DN25274_c0_g1_i1	753.8	-	-
13	DN15360_c0_g1_i1	737.8	tubulin_alpha-2/alpha-4_chain	0
14	DN24725_c0_g1_i1	719.8	-	-
15	DN31074_c0_g1_i1	681.6	complement C1q-like protein 4	2.00E-11
16	DN8976_c0_g1_i1	671.1	Calmodulin-like_protein_5	5.32E-17
17	DN16060_c1_g2_i2	422.7	-	-
18	DN12949_c0_g1_i1	409.6	complement C1q and tumor necrosis factor-related protein	2.00E-09
19	DN14463_c0_g1_i2	340.0	-	-
20	DN15231_c0_g1_i1	339.9	ShK domain-like	2.50E-08
21	DN9823_c0_g1_i1	324.8	-	-
22	DN10028_c0_g1_i1	306.9	peptidyl-prolyl_cis-trans_isomerase_H-like	1.39E-88
23	DN16912_c0_g2_i1	284.9	-	-
24	DN40628_c0_g1_i1	283.4	Arginase family	1.40E-74
25	DN1729_c0_g1_i2	273.8	Conopressin/neurophysin	6.08E-50
26	DN38288_c0_g1_i1	263.0	Lectin C-type domain	4.50E-11
27	DN44922_c0_g1_i1	260.7	peptidyl-prolyl_cis-trans_isomerase_H-like	1.8E-53
28	DN12466_c0_g1_i1	255.0	-	-
29	DN16912_c0_g2_i2	249.5	-	-
30	DN9680_c0_g1_i1	248.1	-	-
31	DN3595_c0_g1_i1	245.2	-	-
32	DN1088_c0_g1_i1	245.1	zinc_metalloproteinase_nas-13-like_isoform_X1	2.43E-70
33	DN6231_c0_g1_i3	203.0	-	-
34	DN7712_c2_g1_i2	179.0	macrophage mannose receptor 1 isoform X1 (Lectin C-type domain)	5.00E-22 (1.80E-19)
35	DN12167_c0_g2_i1	145.2	-	-
36	DN43537_c0_g1_i1	140.8	NIPSNAP	1.10E-17
37	DN12695_c0_g1_i3	139.8	sodium-dependent_phosphate_transport_protein_2A-like	0
38	DN6981_c0_g1_i1	136.9	-	-
39	DN37506_c0_g1_i1	135.5	-	-
40	DN16674_c0_g1_i1	133.1	Cysteine-rich secretory protein family	1.70E-24
41	DN28573_c0_g2_i1	132.9	macrophage mannose receptor 1-like (C-type domain)	9.00E-11 (3.40E-13)
42	DN1648_c0_g2_i2	129.9	-	-
43	DN11986_c0_g2_i2	128.9	ShK domain-like	7.20E-07
44	DN7129_c0_g1_i1	128.1	-	-
45	DN9623_c0_g1_i1	101.2	macrophage mannose receptor (Lectin C-type domain)	5E-23 (1.7E-20)
46	DN4247_c2_g1_i1	101.0	-	-
47	DN930_c0_g1_i1	100.1	-	-
48	DN80054_c0_g1_i1	96.4	Apolipophorin-III precursor	5.00E-12
49	DN27921_c0_g1_i1	95.7	cysteine-rich_venom_protein_pseudechetoxin-like_isoform	3.67E-54
50	DN10164_c1_g1_i1	89.7	C-type domain	4.40E-19

Table 3-2. The top 50 list of proteins detected from the isolated cnidosacs of *P. semperi* by proteomic analysis, arranged in the order of protein quantity.

Rank	Accession	SignalP	Amount (fmol)	Annotation
1	DN9592_c0_g2_i2	×	19834.91	actin,_adductor_muscle
2	DN3615_c1_g1_i1	×	5830.31	actin,_adductor_muscle
3	DN44358_c0_g1_i1	×	4345.71	CENP-T histone fold
4	DN12731_c0_g1_i5	×	3862.929	myosin_heavy_chain,_striated_muscle-like
5	DN92931_c0_g1_i1	×	3250.91	Core histone H2A/H2B/H3/H4
6	DN21256_c0_g1_i1	○	2971.806	collagen_alpha-5(VI)_chain-like
7	DN4790_c1_g1_i1	×	2141.688	actin,_adductor_muscle
8	DN5887_c0_g1_i1	×	2127.242	paramyosin-like_isoform_X1
9	DN9056_c0_g1_i2	×	1829.571	Intermediate filament protein
10	DN20926_c1_g3_i2	×	1617.053	tubulin_beta_chain-like
11	DN1328_c0_g1_i1	×	1396.179	histone_H2A.V
12	DN9592_c0_g2_i1	×	1185.566	actin,_cytoplasmic
13	DN20926_c1_g5_i1	×	1163.07	Tubulin/FtsZ family, GTPase domain
14	DN62598_c0_g1_i1	×	1141.046	histone_H3
15	DN7730_c2_g4_i4	×	984.678	Tubulin/FtsZ family, GTPase domain
16	DN8280_c0_g1_i1	×	922.5421	arginine_kinase-like
17	DN20926_c1_g1_i2	×	836.9141	tubulin_beta_chain-like
18	DN42173_c0_g1_i4	×	826.027	elongation_factor_1-alpha-like
19	DN11996_c0_g1_i2	×	791.934	peroxiredoxin-5,_mitochondrial-like
20	DN24487_c0_g1_i2	×	650.944	ras-related protein Rab-7a
21	DN31991_c0_g2_i1	×	601.905	ATP:guanido phosphotransferase
22	DN8720_c0_g2_i5	×	538.368	Calponin homology (CH) domain
23	DN26959_c0_g2_i1	×	486.8506	-
24	DN9270_c1_g1_i1	×	485.019	transgelin-2-like
25	DN13772_c0_g1_i1	×	458.487	glutamate_receptor_1-like
26	DN10000_c0_g1_i4	○	450.581	cartilage_matrix_protein-like
27	DN47744_c0_g1_i1	○	425.661	collagen_alpha-2(IV)_chain-like
28	DN26959_c0_g1_i1	×	421.9597	-
29	DN12502_c0_g1_i1	×	418.083	myosin_essential_light_chain,
30	DN3646_c1_g2_i1	×	417.491	-
31	DN1116_c0_g1_i1	×	415.358	Intermediate filament protein
32	DN5993_c0_g1_i3	×	414.456	collagen_alpha-3(VI)_chain-like_isoform_X11
33	DN5993_c0_g1_i2	×	390.271	Cartilage_matrix_protein
34	DN20926_c1_g4_i1	×	369.6633	tubulin_beta_chain-like
35	DN12507_c0_g1_i2	×	368.545	ATP_synthase_subunit_beta
36	DN5506_c0_g2_i1	×	351.567	-
37	DN28386_c0_g1_i1	×	351.5654	actin,_cytoplasmic-like
38	DN4817_c0_g1_i1	○	329.897	collagen_alpha-1(IV)_chain_isoform_X1
39	DN20621_c0_g1_i1	×	318.724	voltage-dependent_anion-selective_channel_protein
40	DN3003_c0_g2_i6	×	315.1899	Tropomyosin
41	DN20063_c0_g1_i1	×	314.3553	-
42	DN13268_c2_g1_i1	×	311.433	ATP_synthase_subunit_alpha
43	DN9902_c0_g2_i1	×	308.398	alpha-actinin,_sarcomeric-like_isoform_X2
44	DN49067_c0_g1_i1	×	293.38	cofilin
45	DN6249_c1_g1_i3	○	283.251	collagen_alpha-5(VI)_chain-like_isoform_X2
46	DN5998_c0_g2_i1	×	274.396	protein_singed-like
47	DN14549_c0_g1_i2	×	272.497	peptidyl-prolyl_cis-trans_isomerase-like
48	DN3187_c0_g1_i1	○	271.801	macrophage mannose receptor 1
49	DN6434_c2_g1_i2	×	258.705	protein_epsilon-like_isoform_X2
50	DN18003_c1_g1_i4	○	256.305	carbonic_anhydrase_13-like

Table 3-3. The top 50 list of proteins detected from the secretion extruded from the cerata of *P. semperi* by proteomic analysis, arranged in the order of protein quantity.

Rank	Accession	SignalP	Amount (fmol)	Annotation
1	DN9056_c0_g1_i2	×	5851.527	Intermediate filament protein
2	DN86606_c0_g1_i1	×	2702.901	-
3	DN9592_c0_g2_i2	×	2111.596	actin,_adductor_muscle
4	DN15360_c0_g1_i1	×	2083.915	Tubulin_alpha-2/alpha-4_chain
5	DN20926_c1_g1_i2	×	1275.287	Tubulin_beta_chain-like
6	DN85806_c0_g1_i1	○	1172.346	Phospholipase A2
7	DN10480_c0_g1_i1	×	1165.143	-
8	DN51719_c0_g1_i1	×	1027.017	Tubulin_beta_chain
9	DN20926_c1_g5_i1	×	580.0167	Tubulin/FtsZ family, GTPase domain
10	DN1858_c0_g1_i1	×	562.849	ras-related protein Rab-35 isoform X1
11	DN92931_c0_g1_i1	×	411.124	Core histone H2A/H2B/H3/H4
12	DN5887_c0_g1_i1	×	381.277	paramyosin-like_isoform_X1
13	DN9592_c0_g2_i1	×	351.9714	actin,_cytoplasmic
14	DN1116_c0_g1_i1	×	331.632	Intermediate filament protein
15	DN20926_c1_g4_i1	×	292.0027	Tubulin_beta_chain-like
16	DN3615_c1_g1_i1	×	270.9319	actin,_adductor_muscle
17	DN77_c0_g1_i5	×	251.163	mantle_muscle-like_isoform_X1
18	DN5763_c0_g1_i4	×	222.021	-
19	DN16419_c0_g1_i1	×	219.027	-
20	DN12731_c0_g1_i5	×	218.0383	myosin_heavy_chain,_striated_muscle-like
21	DN8181_c0_g2_i2	×	203.973	calmodulin-like isoform X1
22	DN13484_c0_g1_i1	○	194.955	protein_disulfide-isomerase-like_isoform_X1
23	DN46908_c0_g1_i2	○	192.806	NPC intracellular cholesterol transporter 2
24	DN60411_c0_g1_i1	○	189.81	-
25	DN11996_c0_g1_i2	×	185.728	peroxiredoxin-5,_mitochondrial-like
26	DN21076_c1_g1_i4	○	184.337	probable_chitinase_10
27	DN79916_c0_g1_i1	×	180.851	Tubulin/FtsZ family, GTPase domain
28	DN1307_c0_g1_i1	×	179.511	cytochrome_P450_26A1-like
29	DN13570_c0_g1_i1	×	175.554	peroxiredoxin-6-like
30	DN12507_c0_g1_i2	×	171.016	ATP_synthase_subunit_beta
31	DN28386_c0_g1_i1	×	167.3393	actin,_cytoplasmic-like
32	DN3739_c1_g1_i1	×	159.666	glutathione-independent_glyoxalase
33	DN43475_c0_g1_i1	○	157.065	-
34	DN14549_c0_g1_i2	×	156.45	peptidyl-prolyl_cis-trans_isomerase-like
35	DN12502_c0_g1_i1	×	151.205	myosin_essential_light_chain
36	DN62598_c0_g1_i1	×	145.008	histone_H3
37	DN91137_c0_g1_i1	×	140.805	V-type_proton_ATPase_subunit_E
38	DN4790_c1_g1_i1	×	137.7668	actin,_adductor_muscle
39	DN1328_c0_g1_i1	×	133.7235	histone_H2A.V
40	DN79991_c0_g1_i1	×	123.94	-
41	DN42173_c0_g1_i4	×	119.722	elongation_factor_1-alpha-like
42	DN7730_c2_g4_i4	×	116.2797	Tubulin/FtsZ family, GTPase domain
43	DN20284_c0_g3_i1	×	111.305	Glyceraldehyde 3-phosphate dehydrogenase
44	DN3444_c0_g1_i2	×	101.483	Tubulin/FtsZ family, GTPase domain
45	DN66248_c0_g1_i1	×	100.8872	Tubulin^Tubulin/FtsZ family, GTPase domain
46	DN10241_c0_g3_i1	×	94.543	superoxide_dismutase_[Cu-Zn]-like
47	DN20926_c1_g3_i2	×	92.895	Tubulin_beta_chain-like
48	DN13268_c2_g1_i1	×	92.8628	ATP_synthase_subunit_alpha
49	DN7730_c1_g1_i2	×	88.2105	Tubulin_alpha-1A_chain-like
50	DN1622_c0_g1_i7	×	85.92	Carb_anhydrase

GENERAL DISCUSSION

Here, finally, on the basis of my findings in combination with previous knowledge, I would like to discuss the biological function and evolution of the dorsal cerata, the cnidosac and the cnidophage that play central roles in kleptocnida observed in *P. semperi* and other sea slugs. **Figure GD-1** shows the schematic phylogeny of aeolidid and allied cladobranchian families on which kleptocnida-related traits are mapped (Goodheart et al. 2017; Goodheart et al. 2018). The dorsal cerata, in which the cnidosac exists and kleptocnida occurs, are diverse in morphology and number, found not only in the Aeolidida but also in the other groups, and thus likely to have evolved and lost multiple times in the evolutionary course of the Cladobranchia (Herdman 1890; Kathe 1996).

In this study, I investigated the growth and morphology of the dorsal cerata in *P. semperi* and clarified the developmental patterns of the cerus formation, which made it possible to predict where new cerata are formed. This information was important in investigating the development of the cnidosac, which occurs in newly formed cerata. I showed that the number of cerata increases dramatically as the sea slugs grow, which suggested that bearing more cerata may be important for growth and survival of *P. semperi*. What, then, are biological roles of the dorsal cerata for *P. semperi* and other cladobranchian sea slugs?

As briefly mentioned in Part I, it has been argued that the dorsal cerata of the sea slugs may play such biological roles as enhanced gas exchange by increasing epidermal surface area (Herdman 1890), photosynthesis by harboring symbiotic zooxanthellae (Rudman 1982), and defense against enemies by kleptocnida or other means (Edmunds 2009). It should be noted that a variety of defensive strategies have been reported or suspected for the dorsal cerata of sea slugs. In some cases, the cerata are autotomized upon predatory attacks, thereby enabling escape of the animals at the expense of a part of the dorsal cerata. In other cases, the cerata make the animals less recognizable for predators by the effect of mimicry. There have been reports on glands developing within the cerata that secrete harmful substances against predators (Edmunds 1966). In this context, it seems

plausible, although speculative, that the evolution of the dorsal cerata preceded the evolution of the cnidosac and the original roles of the cerata are likely unrelated to kleptocnida.

Considering that the nematocysts stored within the cnidophages are derived from food cnidarians, the feeding habit of sea slugs may have relevance to the evolution of kleptocnida. For example, it is notable that, while the majority of aeolidid sea slugs feed on cnidarians and possess the cnidosac within the dorsal cerata, some members of the family Fionidae are non-cnidarian feeders and have lost the cnidosac (McDonald and Nybakken 1991; Goodheart et al. 2017) (**Fig. GD-1**). Considering that the nematocysts are encased in thick capsule and contain toxins, it has been argued that aeolidid sea slugs may have originally evolved the cnidosac to store, isolate and dispose the undigested nematocysts at the tip of the cerata (Grosvenor 1903; Martin 2003). In this context, a *Hancockia* species, which is the only known non-aeolidid species with the cnidosac and kleptcnida (see **Fig. GD-1**), is of great interest. In this species, the food-derived nematocysts are first incorporated into the cnidophages, then transported to the cnidosac, and finally digested there in a relatively short period of time (Martin et al. 2009). In aeolidid species, by contrast, the food-derived nematocysts are free within the digestive tract, transported to the tip of the cerata, and incorporated into the cnidophages. Why the nematocysts do not discharge within the digestive tract of the sea slugs is an enigma. It has been argued that the mucus of the sea slugs may have an activity to inhibit the nematocyst discharge, thereby enabling them to feed on cnidarians without injury (Greenwood 2004). Alternatively, it has been proposed that the sea slugs may selectively keep and store immature nematocysts without discharging ability within the cnidosac, where the nematocysts mature and become capable of discharge (Obermann et al. 2012). Here, however, the mechanisms as to how the cnidarian nematocysts can be led to maturity within the molluscan cells are totally unknown.

As described in Part II, by keeping cerata-excised individuals of *P. semperi* without feeding cnidarians, I observed that the cnidophage differentiation occurred in the regenerating ceratal tip even in the absence of nematocyst incorporation, which uncovered that the cnidophage differentiation can proceed autonomously. Here it is notable that, when the experimental animals

with the nematocyst-free cnidosac are fed with cnidarians and subsequently inspected histologically, I will be able to observe the process of nematocyst incorporation into the cnidophages in detail, which I am planning as my next research project. Within the regenerating cnidosacs, I observed that newly formed cnidophages extend pseudopodia-like projections (see **Fig. 2-6**), suggesting the possibility that phagocytotic mechanisms may be involved in the incorporation of the nematocysts into the cnidophages. It is notable that such phagocytosis is seen in kleptoplastic sea slugs, in which the digestive epithelial cells extend protrusions and take up the chloroplasts (Martin et al. 2013). In Part III of this study, I identified that several phagocytosis-related genes and proteins are preferentially expressed in the cnidosac of *P. semperi* (**Table 3-1; Table 3-2**). Future functional studies on such genes and molecules would shed light on the molecular and cellular mechanisms of kleptocnida.

The evolutionary developmental origin of the cnidophage is an intriguing unsolved question. On account of the location at the tip of the digestive glands (see **Fig. 2-1**), it seems plausible that the cnidophage may be derived from the digestive epithelial cells. On the other hand, considering the observations that the cnidophage exhibits phagocytotic cytology (**Fig. 2-6**) and expresses immune- and phagocytosis-related genes (**Table 3-1; Table 3-2**), it is conceivable that the cnidophage may be derived from the hemocytes. Future comprehensive transcriptomic studies on the cnidophage and other cell types of *P. semperi* would provide further insight into this fundamental problem.

REFERENCES

Edmunds M. (1966) Protective mechanisms in the Eolidacea (Mollusca Nudibranchia). J Lin Soc Lond Zool 46: 27–71

Edmunds M (2009) Do nematocysts sequestered by aeolid nudibranchs deter predators? – a background to the debate. J Molluscan Stud 75: 203–205

Goodheart JA, Bazinet AL, Valdés Á, Collins AG, Cummings MP (2017) Prey preference follows phylogeny: evolutionary dietary patterns within the marine gastropod group Cladobranchia (Gastropoda: Heterobranchia: Nudibranchia). BMC Evol Biol 17 1: 1-14

Goodheart JA, Bleidißel S, Schillo D, Strong EE, Ayres DL, Preisfeld A, Collins AG, Cummings MP, Wägele H (2018) Comparative morphology and evolution of the cnidosac in Cladobranchia (Gastropoda: Heterobranchia: Nudibranchia). Front Zool 15 1: 1-18

Greenwood PG, Garry K, Hunter A, Jennings M (2004) Adaptable defense: a nudibranch mucus inhibits nematocyst discharge and changes with prey type. Biol Bull 206: 113–120

Grosvenor G (1903) On the nematocysts of AEolids. Proc R Soc Lond 426–486

Herdman WA (1890) On the structure and functions of the cerata or dorsal papillae in some nudibranchiate Mollusca. Journal of Cell Science 2: 41–64

Kathe J (1996) Phylogenetic systematics and classification of the Sacoglossa (Mollusca, Gastropoda, Opisthobranchia). Phil Trans R Soc Lond B 351: 91–122

Martin R (2003) Management of nematocysts in the alimentary tract and in cnidosacs of the aeolid nudibranch gastropod *Cratena peregrina*. Marine Biology 143: 533–541

Martin R, Heß M, Schrödl M, Tomaschko KH (2009) Cnidosac morphology in dendronotacean and aeolidacean nudibranch molluscs: from expulsion of nematocysts to use in defense? Mar Biol 156: 261–268

Martin R, Walther P, Tomaschko KH (2013) Phagocytosis of algal chloroplasts by digestive gland cells in the photosynthesis-capable slug *Elysia timida* (Mollusca, Opisthobranchia, Sacoglossa). Zoomorphology 132: 253–259

McDonald G, Nybakken J (1991) A preliminary report on a world-wide review of the food of

nudibranchs J Molluscan Studies 57: 61–63

Obermann D, Bickmeyer U, Wägele H (2012) Incorporated nematocysts in *Aeolidiella stephanieae* (Gastropoda, Opisthobranchia, Aeolidoidea) mature by acidification shown by the pH sensitive fluorescing alkaloid Ageladine A. Toxicon 60: 1108–1116

Rudman WB (1982) The taxonomy and biology of further aeolidacean and amerinacean nudibranch molluscs with symbiotic zooxanthellae. Zool J Linn Soc 74: 147-196

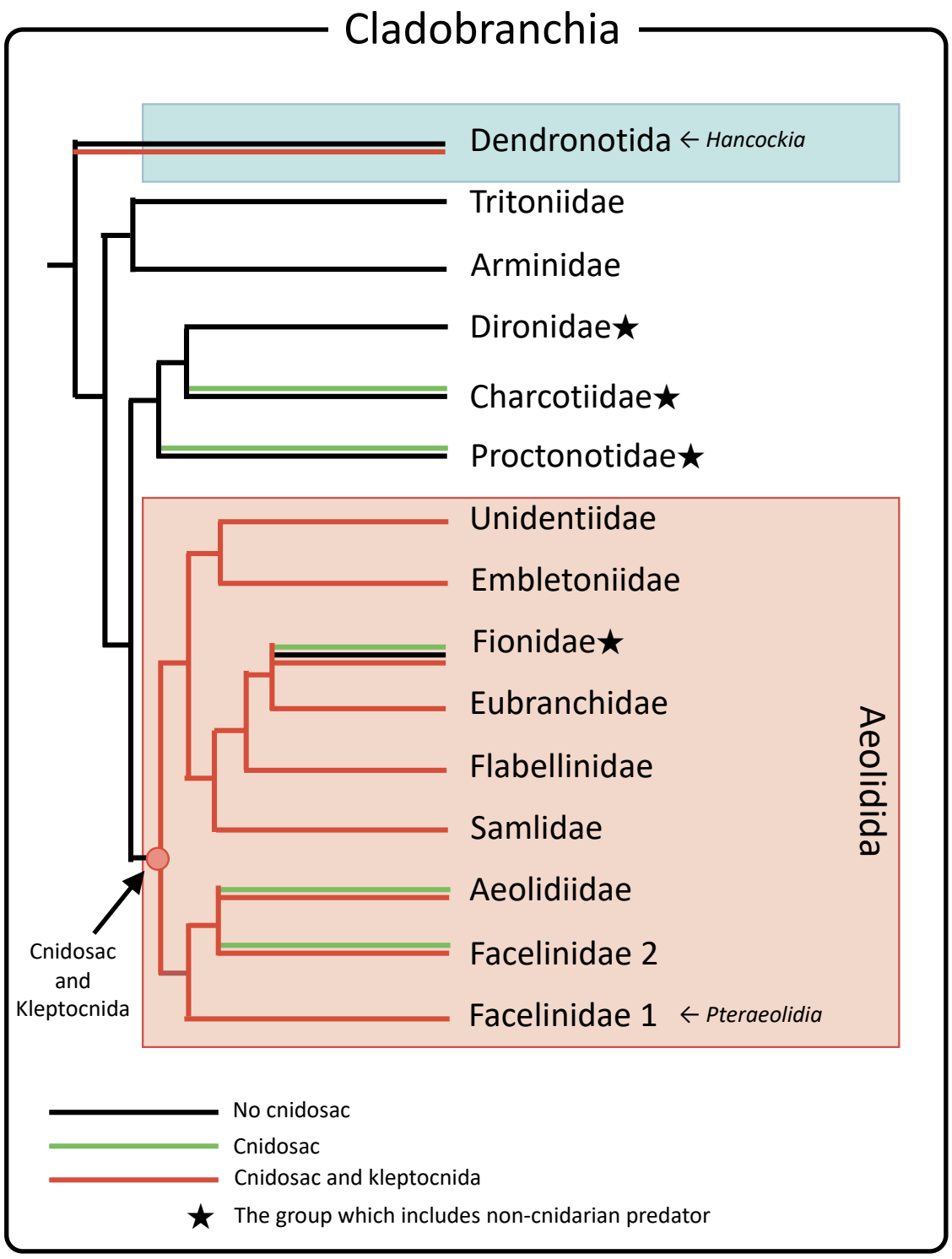

(adapted from Goodheart et al. 2017; 2018)

Fig. GD-1. Schematic phylogeny of aeolidid and allied cladobranchian families (based on Goodheart et al. 2017 and 2018 with modification).

CONCLUDING REMARKS

In Part I of this thesis, I observed and described the development and morphogenesis of *P. semperi* in an unprecedented detail, with special attention to the formation and increase of the dorsal cerata. I demonstrated how the number of cerata is related to the body length, the number of ceratal rows, and the formation of the glove structure in *P. semperi*. On the basis of these observations, I defined and proposed 4 developmental phases of the cerata formation during the growth of *P. semperi* (see **Fig. 1-5**). I also identified that new cerata are formed on the tail of the animals and also on both sides of the glove structures. These results, in particular the sites of new cerata formation, were important and useful for investigating the developmental process of the cnidosac formation, which must proceed in newly formed cerata.

In Part II, by referring to the information of Part I, the developmental and regeneration processes of the cnidosac were investigated in detail. I histologically observed the newly formed cerata on the posterior tip region of the animals and also on both sides of the globe structures, by which the normal developmental process of the cnidosac was described. In addition, by excising the tip of cerata, maintaining the operated animals, and sampling the regenerating cerata periodically, I observed the formation process of the cnidosac within the regenerating cerata. On the basis of these observations, I defined and proposed 5 developmental stages of the cnidosac formation during the formation process of the cerata in *P. semperi* (see **Fig. 2-5**). Furthermore, by transmission electron microscopy, I observed the ultrastructural traits of the cnidophage, thereby uncovering several previously undescribed features including accumulated granules around the incorporated nematocytes within the cnidophage. These results on the detailed developmental and morphogenetic aspects of the cerata, the cnidosac and the cnidophage, the organ, the tissue and the cell for kleptocnida, lay the foundation for future studies on the mechanisms underlying the interesting but enigmatic phenomenon, kleptocnida.

In Part III, in an attempt to understand the molecular mechanisms underpinning kleptocnida, I performed transcriptomic analysis of the kleptocnida-related tissue samples of *P. semperi*, namely the excised ceras tip, in comparison with the other tissue samples like the excised ceras base, the head

tentacle and the oral tentacle. Comparative analysis of the transcriptomic data revealed a number of candidate genes that are highly and preferentially expressed in the tip of cerata where kleptocnida occurs. These candidate genes are dominated by muscle-, cytoskeleton- and collagen-related genes, and also contained immune-related genes and binding- or phagocytosis-related genes, providing structural and functional insights into the cnidosac and the cnidophage. I also performed proteomic analysis of the dissected cnidosacs and the secretion samples squeezed from the ceras tips. The proteomic data were generally concordant with the transcriptomic data. Based on these cnidosac-associated transcriptomic and proteomic data, I argued and speculated how these molecules can potentially be involved in kleptocnida.

In this study, I compiled the morphological, histological, developmental and molecular data toward understanding of the processes and the mechanisms of the unique, bizarre, and interesting biological phenomenon, kleptocnida, using *P. semperi* as a model system. Needless to say, I am still just at the beginning of understanding the mechanisms of kleptocnida, and planning several future projects to be focused on next.

(i) Elucidation of process and mechanism of nematocyst incorporation into cnidophage: Since *P. semperi* is symbiotic with photosynthetic dinoflagellates, the animals can be maintained without food cnidarians under sufficiently illuminated conditions. Therefore, by excising the tip of cerata and keeping the operated animals without feeding, I can obtain the animals with regenerated cerata and cnidosacs that are nematocyst-free. I expect that, when I provide such animals with food cnidarians, I will be able to conveniently monitor the process of nematocyst incorporation into the cnidophage. I would like to investigate what morphological, physiological, transcriptomic and other changes are observed in the cnidophage before and after the nematocyst acquisition.

(ii) Localization and dynamics of cnidosac-associated genes and proteins: By transcriptomic and proteomic analyses, I listed a number of candidate genes and proteins that may be preferentially expressed and functioning in the cnidosac and/or the cnidophage of *P. semperi*. At present, however, it has not been verified whether these candidate molecules are actually expressed and functioning there.

Hence, I will conduct in situ hybridization and immunohistochemistry experiments, thereby identifying the true candidate genes and proteins that are expressed in the cnidosac and/or the cnidophage.

(iii) Functional analysis of cnidosac-associated genes and proteins: When some genes and proteins preferentially expressed in the cnidosac and/or the cnidophage are identified, I would like to perform functional analysis of such genes by, for example, RNAi knockdown of the gene expression. Thus far, no previous studies have reported successful application of such molecular genetic techniques to sea slugs, but I will try to overcome the difficulty and open a new window to look into the enigmatic mechanism of kleptocnida.

ACKNOWLEDGEMENTS

I would particularly like to thank Professors Takema Fukatsu and Toru Miura for guiding my study and valuable advice throughout my doctoral course. Without their guidance and persistent help, this thesis would not have been possible. I appreciate the guidance of experimental techniques and insightful comments by Minoru Moriyama. Junpei Shinji's constructive comments and guidance in the analyses were of enormous help to me. I am grateful to Masanori Okanishi, Hisanori Kohtsuka, Mamoru Sekifuji, Michiyo Kawabata, Miho Kyokuwa and Mayuko Nakamura for their assistance in my field sampling. I was supported and encouraged by all the members of the Misaki Marine Biological Station, the University of Tokyo, and the Symbiotic Evolution and Biological Functions Research Group, the National Institute of Advanced Industrial Science and Technology (AIST). I was supported by the JSPS Fellowship for Young Scientists and the Grant-in-Aid for JSPS Fellows (20J11297).